

AD-A137 103

FABRICATION AND EVALUATION OF CHIRPED GRATING LENSES IN  
LITHIUM NIOBATE W. (U) CALIFORNIA UNIV SAN DIEGO LA  
JOLLA DEPT OF ELECTRICAL ENGINEER. S FOROUHAR ET AL.

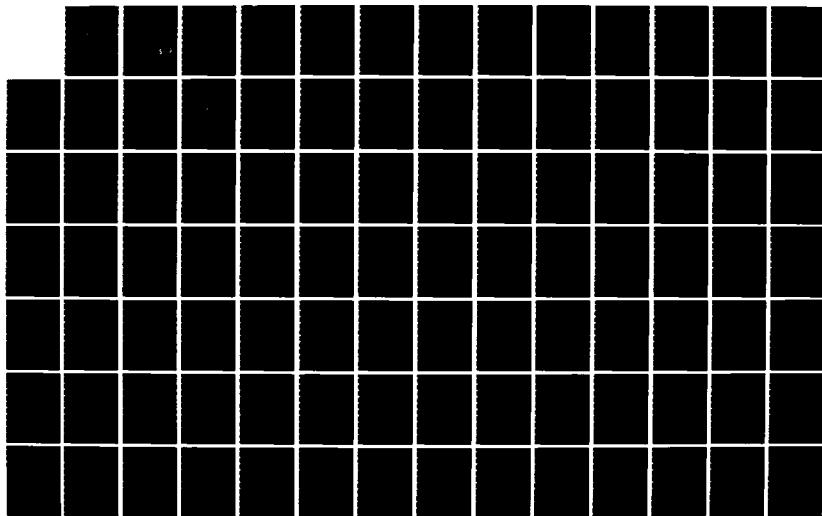
1/2

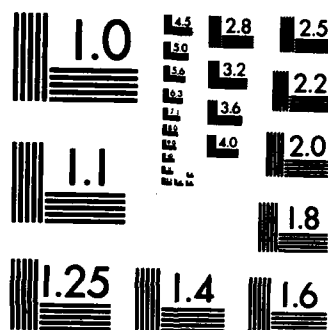
UNCLASSIFIED

01 OCT 83 AFOSR-TR-83-1314 AFOSR-80-0037

F/G 20/6

NL





MICROCOPY RESOLUTION TEST CHART  
NATIONAL BUREAU OF STANDARDS-1963-A

UNCLASSIFIED

Unclassified

2

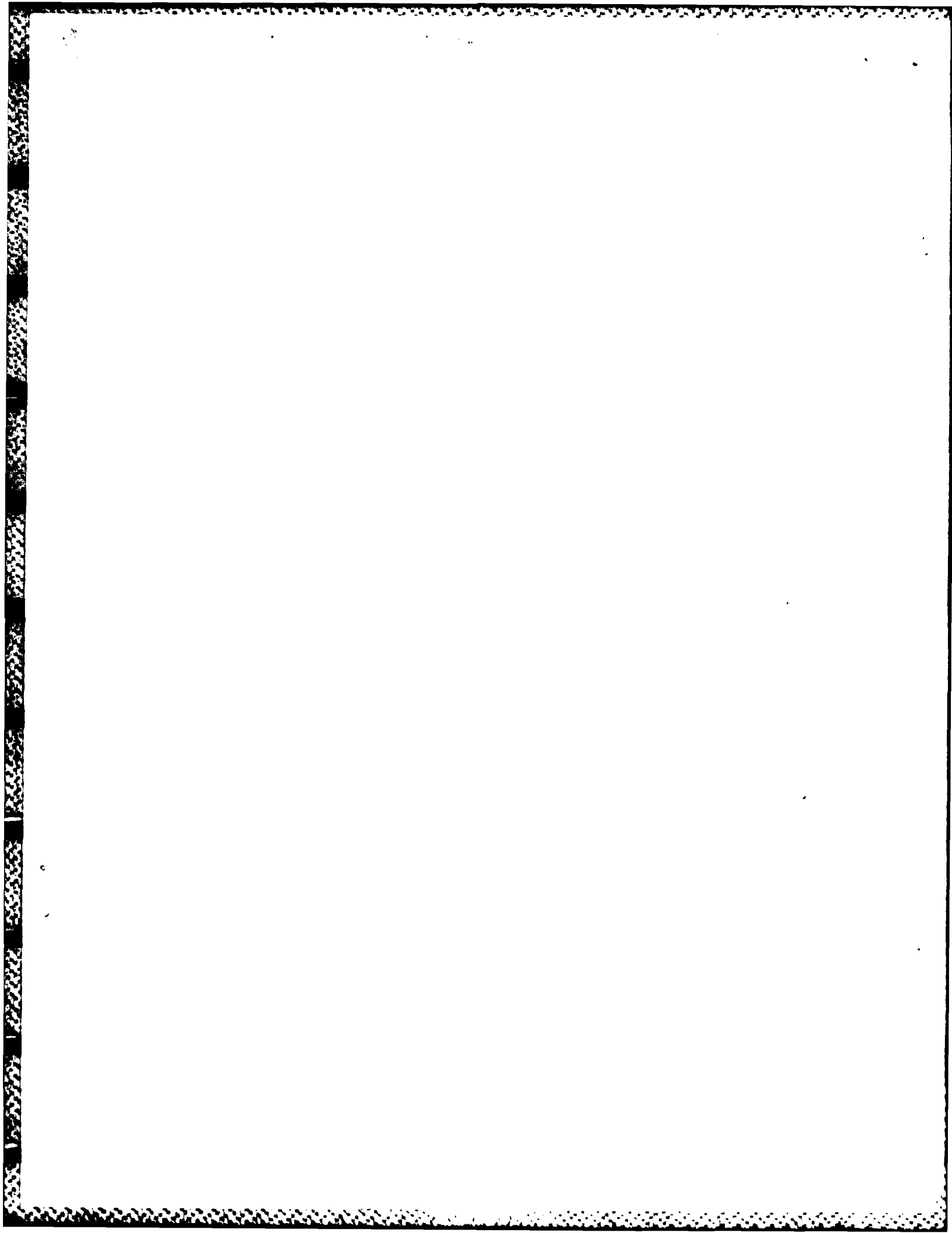
SECURITY CLASSIFICATION OF THIS PAGE (When Data Entered)

REPORT DOCUMENTATION PAGE		READ INSTRUCTIONS BEFORE COMPLETING FORM
1. REPORT NUMBER <b>AFOSR-TR- 83-1314</b>	2. GOVT ACCESSION NO. <b>AD-A137103</b>	3. RECIPIENT'S CATALOG NUMBER
TITLE (and Subtitle) <b>Fabrication and Evaluation of Chirped Grating Lenses in Lithium Niobate Waveguides</b>		5. TYPE OF REPORT & PERIOD COVERED <b>Interim Report 1 June 82 - 31 Sept 83</b>
AUTHOR(s) <b>Forouhar Chang Warren Xin-Lu</b>		6. PERFORMING ORG. REPORT NUMBER
PERFORMING ORGANIZATION NAME AND ADDRESS <b>Department of Electrical Engineering &amp; Computer Sciences University of California San Diego La Jolla, CA 92093</b>		8. CONTRACT OR GRANT NUMBER(s) <b>AFOSR-80-0037</b>
1. CONTROLLING OFFICE NAME AND ADDRESS <b>Air Force Office of Scientific Research/NE Building 410 Bolling AFB, DC 20332</b>		10. PROGRAM ELEMENT, PROJECT, TASK AREA & WORK UNIT NUMBERS <b>61102F 2305/B1</b>
4. MONITORING AGENCY NAME & ADDRESS (if different from Controlling Office)		12. REPORT DATE <b>Oct 1, 1983</b>
		13. NUMBER OF PAGES <b>161</b>
		15. SECURITY CLASS. (of this report) <b>Unclassified</b>
		15a. DECLASSIFICATION/DOWNGRADING SCHEDULE
16. DISTRIBUTION STATEMENT (of this Report)  <b>Approved for public release; distribution unlimited.</b>		
17. DISTRIBUTION STATEMENT (of the abstract entered in Block 20, if different from Report)		
18. SUPPLEMENTARY NOTES		
19. KEY WORDS (Continue on reverse side if necessary and identify by block number)		
20. ABSTRACT (Continue on reverse side if necessary and identify by block number) <b>Theoretical methods have been formulated for the design and analysis of chirped grating lenses on planar optical waveguides. Various fabrication techniques such as deposition of high index titanium dioxide films and reactive ion milling of LiNbO<sub>3</sub> have been developed to create low-loss phase shift pads on Ti-indiffused LiNbO<sub>3</sub> waveguides. Etched and deposited groove chirped grating lenses have been successfully fabricated and evaluated for the first time on Ti-indiffused LiNbO<sub>3</sub> waveguides. A throughput efficiency of 85% for TiO<sub>2</sub> deposited grooves and 80% for etched grooves has been measured</b>		

AD A 137103

DTIC FILE COPY

DTIC  
ELEC  
JAN 20 1984  
S  
E



UNCLASSIFIED

AFOSR-TR- 83-1314

SECURITY CLASSIFICATION OF THIS PAGE(When Data Entered)

Unclassified

20.

for some lenses. It has been determined that due to the properties of Ti-indiffused LiNbO<sub>3</sub> waveguides, it is difficult to achieve high efficiency with large angular field of view (i.e. more than two degrees) chirped grating lenses on such waveguides. The limitations are caused primarily due to the closeness of the mode index and the substrate index in single mode Ti-indiffused waveguides. To improve the grating lens performance, two alternative waveguides in LiNbO<sub>3</sub> have been investigated that have larger mode index. The feasibility of using Nb<sub>2</sub>O<sub>5</sub> transition waveguide to interconnect two separate sections of Ti-indiffused waveguides has been demonstrated with a total insertion loss of 0.8 dB. The chirped grating lenses fabricated on top of such a waveguide by reactive ion beam etching have 85% throughput efficiency and more than four degrees angular field of view. Ion-exchanged LiNbO<sub>3</sub> waveguides have been investigated as the second alternative. Chirped grating lenses with diffraction efficiency of 75% and three degrees angular field of view have been fabricated by a second ion exchanged process in these waveguides. The fabrication techniques, the theoretical methods and the materials investigated are not limited to the chirped grating lenses and may also be used in the design and fabrication of other integrated optical components.

Accession For	
NTIS GRA&I	<input checked="" type="checkbox"/>
DTIC TAB	<input type="checkbox"/>
Unannounced	<input type="checkbox"/>
Justification	
By	
Distribution/	
Availability Codes	
Dist	Avail and/or Special
A-1	



Unclassified

SECURITY CLASSIFICATION OF THIS PAGE(When Data Entered)

2305 31

AFOSR-TR- 83 - 1314

UNIVERSITY OF CALIFORNIA

San Diego

Fabrication and Evaluation of  
Chirped Grating Lenses in Lithium Niobate Waveguides

*Interim*  
Technical Report  
October 1, 1983

by

Siamak Forouhar, Christopher Warren, Ron Xin-Lu  
and William S.C. Chang

Department of Electrical Engineering and Computer Sciences  
C-014  
University of California, San Diego  
La Jolla, CA 92093

Work supported in part by AFOSR  
and TRW subcontract P23817RX35

- 80-0037

84 01 19 074

Approved for public release;  
distribution unlimited.

**Fabrication and Evaluation of  
Chirped Grating Lenses in Lithium Niobate Waveguides**

**ABSTRACT**

Theoretical methods have been formulated for the design and analysis of chirped grating lenses on planar optical waveguides. Various fabrication techniques such as deposition of high index titanium dioxide films and reactive ion milling of  $\text{LiNbO}_3$  have been developed to create low-loss phase shift pads on Ti-indiffused  $\text{LiNbO}_3$  waveguides. Etched and deposited groove chirped grating lenses have been successfully fabricated and evaluated for the first time on Ti-indiffused  $\text{LiNbO}_3$  waveguides. A throughput efficiency of 85% for  $\text{TiO}_2$  deposited grooves and 80% for etched grooves has been measured for some lenses. It has been determined that due to the properties of Ti-indiffused  $\text{LiNbO}_3$  waveguides, it is difficult to

AIR FORCE OFFICE OF SCIENTIFIC RESEARCH  
NOTICE OF TECHNICAL REPORT  
This technical report is approved for public release and distribution is unlimited.  
MATTHEW J. KERPER  
Chief, Technical Information Division

achieve high efficiency with large angular field of view (i.e. more than two degrees) chirped grating lenses on such waveguides. The limitations are caused primarily due to the closeness of the mode index and the substrate index in single mode Ti-indiffused waveguides.

To improve the grating lens performance, two alternative waveguides in  $\text{LiNbO}_3$  have been investigated that have larger mode index.

The feasibility of using  $\text{Nb}_2\text{O}_5$  transition waveguide to interconnect two separate sections of Ti-indiffused waveguides has been demonstrated with a total insertion loss of 0.8 dB. The chirped grating lenses fabricated on top of such a waveguide by reactive ion beam etching have 85% throughput efficiency and more than four degrees angular field of view.

Ion-exchanged  $\text{LiNbO}_3$  waveguides have been investigated as the second alternative. Chirped grating lenses with diffraction efficiency of 75% and three degrees angular field of view have been fabricated by a second ion exchanged process in these waveguides.

The fabrication techniques, the theoretical methods and the materials investigated are not limited to the chirped grating lenses and may also be used in the design and fabrication of other integrated optical components.

## TABLE OF CONTENTS

	Page
Abstract .....	1
CHAPTER I .....	1
Introduction .....	2
CHAPTER II .....	11
Perturbation and Iterative Perturbation Analysis of Linearly Chirped Grating Lenses of Medium Q in Dielectric Waveguides .....	12
CHAPTER III .....	46
Performance and Limitations of Chirped Grating Lenses on Ti-indiffused LiNbO <sub>3</sub> Planar Waveguides .....	47
CHAPTER IV .....	83
Chirped Grating Lenses on Nb <sub>2</sub> O <sub>5</sub> Transition Waveguides ....	84
CHAPTER V .....	107
Double Ion Exchanged Chirp Grating Lens in Lithium Niobate Waveguides .....	108
CHAPTER VI .....	121
Conclusion .....	122
CHAPTER VII .....	129
Appendix I .....	130
Appendix II .....	145

To the Memory of my  
Father

## TABLE OF CONTENTS

	Page
Acknowledgements .....	vi
Vita, Publications and Field of Study .....	vii
Abstract .....	viii
CHAPTER I .....	1
Introduction .....	2
CHAPTER II .....	11
Perturbation and Iterative Perturbation Analysis of Linearly Chirped Grating Lenses of Medium Q in Dielectric Waveguides .....	12
CHAPTER III .....	46
Performance and Limitations of Chirped Grating Lenses on Ti-indiffused LiNbO <sub>3</sub> Planar Waveguides .....	47
CHAPTER IV .....	83
Chirped Grating Lenses on Nb <sub>2</sub> O <sub>5</sub> Transition Waveguides...	84
CHAPTER V .....	107
Double Ion Exchanged Chirp Grating Lens in Lithium Niobate Waveguides .....	108
CHAPTER VI .....	121
Conclusion .....	122
CHAPTER VII .....	129
Appendix I .....	130
Appendix II .....	145

## ACKNOWLEDGEMENTS

The completion of this dissertation would not be possible without contributions of several people. For their technical as well as moral support I will always be grateful.

My sincere thanks to Professor William S. C. Chang for his patience, guidance and encouragement in the supervision of this research project. His guidance had the greatest influence in the progress of my research.

Special thanks is extended to Jean Marc Delavaux for his technical assistance and useful discussions. All the grating masks used for my research were also fabricated by him.

Thanks to Karen K. Sullivan for the competent way in which she typed the manuscript.

Last and most, I thank my wife for her patience, tolerance and moral support.

This research was supported in part by AFOSR Grant No. 80-0037 with the University of California, San Diego, and by Air Force Avionic Laboratory Contract No. F33615-82-C-1751 with TRW Technology Research Center and University of California, San Diego.

CHAPTER I

## 1. INTRODUCTION

Integrated optical guided wave components have important applications in many logic and signal processing systems, such as the rf spectrum analyzer and high speed analog-to-digital converters [1,2]. In these applications, the performance of guided wave components is potentially superior to that of electronic components because of their fast response and parallel processing capabilities. In addition, the guided wave components are also superior to the conventional bulk optical components because of their ruggedness and low drive power consumption.

In order to realize the majority of the optical guided wave systems in planar configuration, high quality thin film waveguide lenses are required to control the shape of the guided wave beam, i.e., for imaging, focusing or Fourier analyzing.

Extensive effort has been devoted to the design and improvement of the quality of guided wave optical lenses in the past few years [3-7]. As a result, diffraction-limited guided wave optical lenses have been fabricated using a semi-planar technology for thin film Luneberg lenses [7] and a bulk optics technology for geodesic lenses [8] (Figures 1 and 2). However, there are difficulties in the geodesic lens technology because its fabrication involves the precise positioning of tools and because its focusing properties are dependent on processing variations. The Luneberg lens is applicable only to the combination of relatively high index films on low refractive index waveguides whereas the geodesic lens requires aberration correction. These problems may be overcome by employing

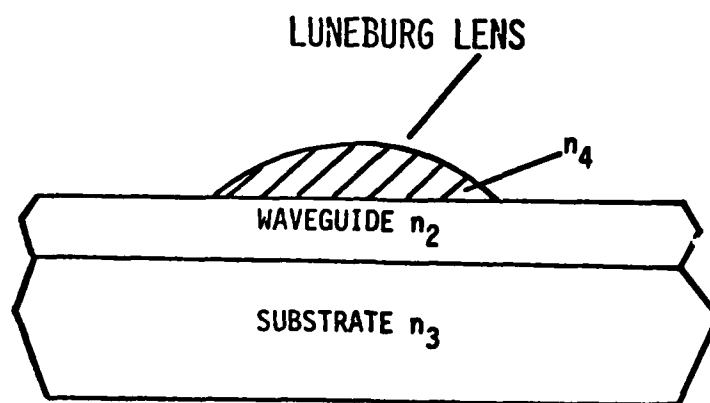


Figure 1. Illustration of an Integrated Optic Luneburg Lens

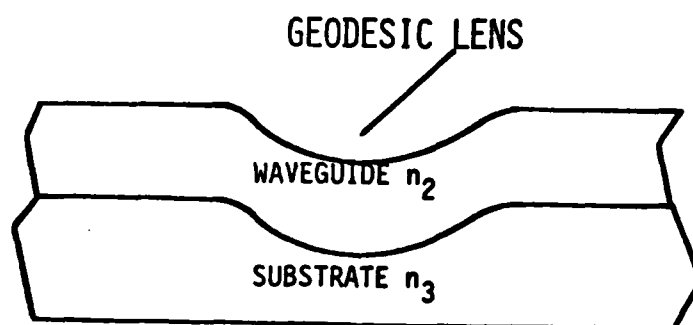


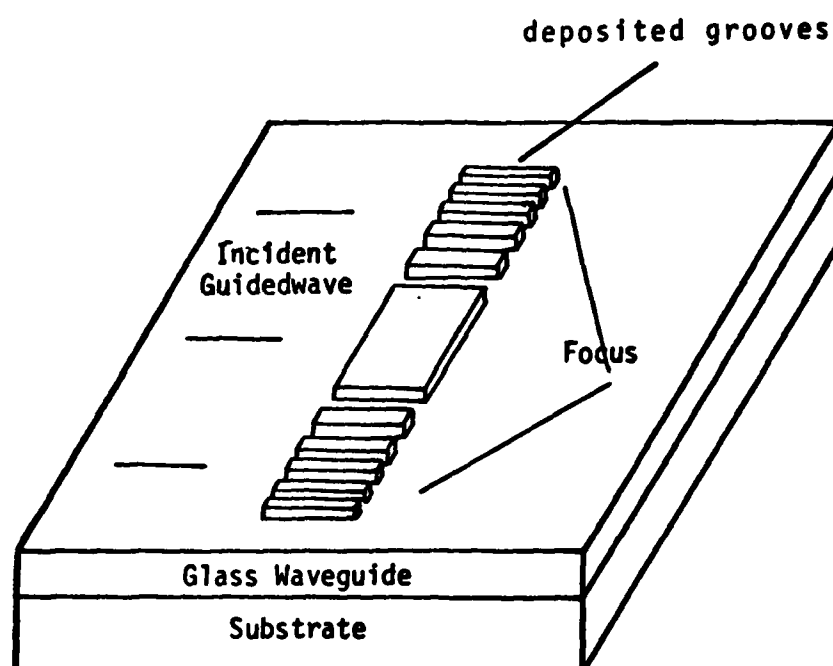
Figure 2. Illustration of an Integrated Optics Geodesic Lens

photo-lithographic or electron-lithographic techniques for a new family of planar grating lenses for guided wave optics [9-12].

Photo-lithographically-compatible guided wave optical lenses already have been fabricated on low refractive index glass waveguides and include the Fresnel phase and Bragg diffraction chirped grating lenses [9,10], illustrated in Figures 3 and 4. However, for some signal processing applications such as rf spectrum analysis, it is necessary to fabricate grating lens structures on Ti-indiffused  $\text{LiNbO}_3$  waveguides that have large acousto-optic and electro-optic coefficients. Questions have been raised concerning the performance of diffraction grating lenses (e.g., the maximum available throughput efficiency, the maximum angular field of view, and the scattering effects of different fabrication techniques) on high index Ti-indiffused  $\text{LiNbO}_3$  waveguides. We have, therefore, devoted significant effort to investigating theoretically and experimentally the performance of chirped grating lenses on Ti-indiffused  $\text{LiNbO}_3$  waveguides.

The role of the theoretical work was (a) to analyze the diffraction properties, (b) to study the effects of the design parameters on the grating lens performance, and (c) to interpret the experimentally measured results. In this regard, three methods have been formulated:

1. A perturbation analysis which is based upon the Green's function (Chapter 2). This analysis is applicable to thin phase grating structures where the effect of feedback from reversed scattering can be neglected.
2. An iterative perturbation method (Chapter 3) in which



WAVEGUIDE FRESNEL LENS

Figure 3. Illustration of an Integrated Optical Fresnel Lens

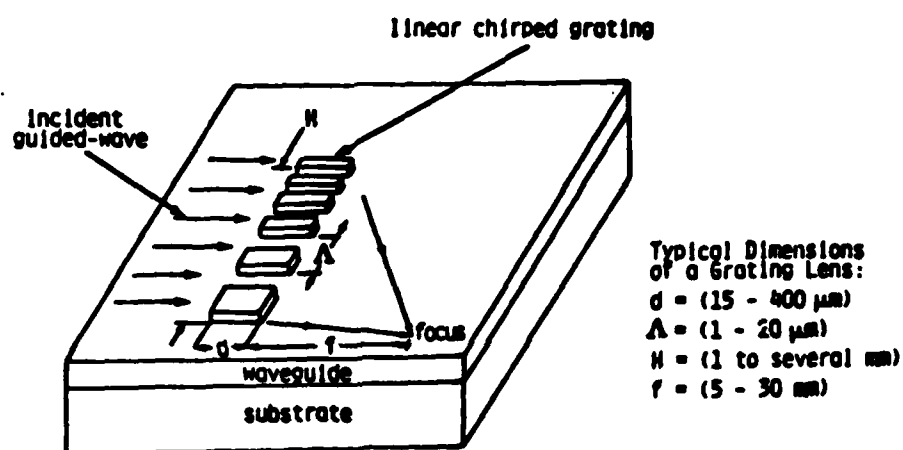


Figure 4. Illustration of an integrated optics chirped grating lens.

a thin section of the grating lens is first analyzed by the perturbation method. The cumulative effect of many thin sections is thereby numerically evaluated by an iterative procedure. This method combines the advantages of the perturbation analysis and the coupled mode analysis.

3. The generalized coupled mode analysis (Appendix 1) which is applicable to situations where volume interaction is restricted only to two dominant guided wave beams. This analysis has been used for the design of different grating lens structures.

However, all the theoretical methods developed assume that there is very little conversion of the guided energy into the radiation modes of the optical waveguide. The experimental conditions under which this assumption is valid partially constitute the limitations of the chirped grating lens performance.

The role of the experimental work was (a) to develop various fabrication technologies and to evaluate different grating lens designs on Ti-indiffused  $\text{LiNbO}_3$  waveguides. This involved the investigation of the various fabrication methods such as the reactive and non-reactive ion milling of  $\text{LiNbO}_3$  materials and the deposition of high index films for creating low-loss phase shift patterns on Ti-indiffused  $\text{LiNbO}_3$  waveguides; (b) to determine the best grating lens performance on Ti-indiffused waveguides; (c) to investigate the limitations that are imposed by the properties of Ti-indiffused waveguides; and (d) to investigate alternative wave-

guide materials on  $\text{LiNbO}_3$  substrates that can improve the performance of the grating lenses and assess the limitations that are imposed by these structures.

As a result of our research effort, high efficiency Bragg diffraction chirped grating lenses on Ti-indiffused  $\text{LiNbO}_3$  waveguides have been realized for the first time. The experimentally measured performance (Chapter 3) of chirped grating lenses on Ti-indiffused  $\text{LiNbO}_3$  waveguides indicates that it is difficult to get both high efficiency and more than two degrees of angular field of view for two reasons: (a) The mode index of Ti-indiffused  $\text{LiNbO}_3$  is close to the substrate index. Therefore, the coupling of energy to the substrate limits the maximum angular field of view or the efficiency of chirped grating lenses. (b) Ti-indiffused  $\text{LiNbO}_3$  waveguides have large mode depth. The large mode depth implies a small coupling coefficient thus requiring long grating grooves which limit the angular field of view.

To improve the grating lens performance, an alternative waveguide in  $\text{LiNbO}_3$  other than Ti-indiffused is needed that has a larger mode index and a smaller mode depth. If Ti-indiffused  $\text{LiNbO}_3$  must be used for other signal processing functions, such as acousto-optic interaction in the rf spectrum analyzer, the alternative waveguide may be used as a transition waveguide interconnecting two sections of Ti-indiffused regions for the grating lens fabrication. As an alternative approach to improve the performance of chirped grating lenses on Ti-indiffused  $\text{LiNbO}_3$ , the feasibility of such interconnections on  $\text{LiNbO}_3$  substrates using  $\text{Nb}_2\text{O}_5$  films were investigated (Chapter 4).

Proton-exchanged  $\text{LiNbO}_3$  waveguides may also be an alternative to improve the performance of chirped grating lenses. The performance of chirped grating lenses on such waveguides were investigated. The results are presented in Chapter 5.

Conclusions and suggestions for future research are presented in Chapter 6. Finally, two appendixes conclude the dissertation. In the first appendix, the design and analysis of chirped grating lenses using the generalized coupled mode theory is described. In the second appendix, the fabrication of grating structures on  $\text{LiNbO}_3$  by reactive ion beam etching and  $\text{TiO}_2$  deposition is discussed.

## References - Chapter I

1. H. F. Taylor, *Proc. IEEE*, 63, 1524 (1976).
2. M. C. Hamilton, D. S. Wille and W. J. Micelli, "An Integrated Optical rf Spectrum Analyzer," *Proc. of IEEE Ultrasonics Symp.*, New York, 218 (1976).
3. W. H. Southwell, *Opt. Soc. Am.*, 67, 1293 (1977).
4. C. M. Verber, D. W. Vahey and V. W. Wood, *Appl. Phys. Lett.*, 28, 514 (1976).
5. D. B. Anderson, R. L. Davis, J. T. Boyd and R. R. August, *IEEE J. Quantum Electron.*, QE-13, 275 (1977).
6. G. E. Betts and G. E. Marx, *Appl. Optics*, 17, 3969 (1978).
7. S. K. Yao, D. B. Anderson, R. R. August, B. R. Youmans and C. M. Dania, *Appl. Optics*, 18, 4067 (1979).
8. B. Chen, T. R. Ranganath, T. R. Joseph and J. Y. Lee, "Progress on the Development of Integrated Optic Spectrum Analyzer," *Top. Mtg. on Integrated and Guided Wave Optics*, Incline Village, Nevada (1980).
9. W. S. C. Chang and P. R. Ashley, *IEEE J. Quantum Electron.*, QE-16, 744 (1980).
10. S. K. Yao and D. E. Thompson, *Appl. Phys. Lett.*, Vol. 33, p. 635, (1978).
11. S. Vallete, A. Morque, and P. Mottier, *Electronics Letters*, 18, 13, (1982).
12. G. Hatakoshi and S. Tanaka, *Optics Letters*, 2, 142, (1978).

## CHAPTER II

A Perturbation and Iterative Perturbation Analysis of Linearly  
Chirped Grating Lenses of Medium Q in Dielectric Waveguides

by

Siamak Forouhar and William S. C. Chang

University of California, San Diego

Department of Electrical Engineering and Computer Sciences (C-014)

La Jolla, CA 92093

ABSTRACT

A perturbation and iterative perturbation analysis of linearly chirped quasi-periodic structures of medium Q factor in planar dielectric waveguides has been formulated. This analysis can be used to calculate the diffraction efficiency and the angular field of view of a given linearly chirped grating structure, for a specific incident beam including the effect of higher orders of diffractions. The numerical example of a  $F=10$ ,  $f=10$  m.m.,  $\Lambda_{\min}=2.06$ ,  $\Lambda_{\max}=4.25$  and grating groove length =  $15 \mu\text{m}$  is presented.

## 1. INTRODUCTION

In recent years, a great deal of research has been conducted in the area of optical guided wave propagation in thick curved and chirped gratings to obtain reflection, focusing, collimation, coupling, and Fourier analysis of the guided waves [1-4]. These gratings will also be useful for millimeter wave applications since similar dielectric waveguides are used in that region. In the past, most grating components had constant periodicity; they were used to obtain coupling to the radiation modes or reflection of guided waves by phase-matched interactions [5,6]. Recently, there has been a lot of interest in the use of chirped grating structures for transforming one form of the guided wave beam into another form of guided wave beam. A typical example of a chirped grating lens is illustrated in Figure 1. It has been demonstrated that such lenses could diffract planar guided wave beams into focused beams with experimentally-measured efficiencies up to 90% [2].

The light diffraction properties of chirped and curved gratings have been analyzed to various degrees of accuracy via several approaches. Most of these analyses are based upon a perturbation method or a modification of the plane-wave coupled wave analysis [7,8]. The modified plane-wave coupled mode analysis can only be used to analyze reflectors or structures that have a very limited chirping rate or curvature. Many perturbation methods neglect the feedback effect on the incident beam, hence they cannot be used to analyze volume interactions. Recently, Lin *et al.* [9] developed a generalized two-dimensional coupled mode approach to analyze the volume interaction of a guided wave beam with curved or chirped gratings that may include a limited amount of phase mismatch. In that analysis, higher orders of diffraction were neglected, only two guided wave beams were considered that are

coupled to each other via the chirped linear or curved grating structure. From the analysis of constant periodicity gratings, we know that the negligence of the higher order diffracted beam is permissible provided the Q factor (given by  $2\pi\lambda_g d/\Lambda^2$  where  $\lambda_g$  is the effective wavelength of the guided wave mode and d is the length of the volume interaction and  $\Lambda$  is the periodicity of the grating structure) is sufficiently high. For chirped gratings, a local Q factor may be defined where  $\Lambda$  is the localized periodicity of the grating structure. The generalized coupled mode theory has been found to yield good results for structures that have high local Q factors [10]. However, it cannot be used to analyze structures that have a medium Q factor ( $1 < Q < 10$ ) because it neglects the presence of higher diffraction orders. Curved or chirped gratings of medium Q can have a moderately large angular field of view, thus they are important for applications such as the  $\lambda/\lambda$  spectrum analysis.

We present here an iterative perturbation method suitable to analyze the diffraction properties of linearly chirped grating structures on planar waveguides with medium Q and straight-line (i.e., linear) grating grooves. In this analysis, two principal guided wave beams are coupled back and forth to each other via the chirped grating structure. These two principal beams may have a variety of horizontal variations (i.e., x, y in Figure 1) such as plane, cylindrical or Gaussian waves, but their z variation is always given by the mode profile of the planar waveguide. In addition, there are other high order weak diffracted beams excited by the two principal beams. However, the feedback effect of these higher order diffracted beams into the two principal beams is neglected. The diffraction into the higher order beams is treated as losses of the two principal beams. The diffraction properties of the grating is analyzed by dividing it into a series of thin longitudinal slabs of thickness  $\delta$ , as illustrated in Figure 2. For each longitudinal slab the

complex amplitudes of the two principal guided wave beams emerging from each section are related to the complex amplitude of the two principal beams incident on the slab by a two by two transfer matrix. The elements of each matrix are calculated using a perturbation method which is based upon a Green's function. Effects of the mutual feedback of the two principal beams as well as the losses to the higher order of diffraction are included in such a calculation. The knowledge of the elements of the transfer matrix associated with each slab enables us to calculate the complex amplitudes of the two principal guided wave beams (as well as the efficiency of diffraction) of the complete chirped grating lens by a simple matrix multiplication. The diffraction efficiency is defined as the power into the focused beam divided by the total power incident on the grating structure.

Alferness [11,12] has analyzed the diffraction efficiency of thick constant periodicity gratings by the method of decomposing them into thin slabs. The present work may be looked upon as an extension of his work to gratings that have chirped periodicities and finite length ( $H$ ) and could be illuminated by either plane guided waves or Gaussian or cylindrical guided waves. As pointed out by Alferness, the method of decomposition has very general applicability. Since the effect of higher diffraction orders could be included, there is no need to require strong Bragg effects (i.e., high  $Q$ ). Although the iterative perturbation analysis may be extended to handle the feedback effects of many orders of diffraction by increasing the elements of the transfer matrix for each slab, we have restricted this paper to only the calculation of two principal guided waves that interact with each other. For a relatively small amount of power in each one of the higher order diffracted beams, the power into the higher orders of diffraction after each slab is considered as a loss to the two principal beams and their feedback into the incident and focused waves have been neglected.

## II. THE THEORETICAL FORMULATION

### A. The Waveguide Modes and the Grating Structure

The modes of a dielectric planar waveguide are the solutions of a wave equation of the form:

$$\nabla^2 e + k_0^2 \epsilon e = 0 \quad (1)$$

when an  $\exp(j\omega t)$  time variation is assumed.  $k_0$  is the free space wave number ( $k_0 = 2\pi/\lambda_0$ ). For a lossless isotropic single mode planar waveguide, without any grating structure, we can express the amplitude of the transverse component of the electric field of any guided TE mode by the product of two functions, one describing the vertical variation of the electric field in depth directions (i.e., the  $z$  direction), and the other that describes the horizontal (i.e.,  $x$  and  $y$ ) variation of the electric field in the plane of propagation. Therefore,

$$e = E(z) \phi(x, y) \quad (2)$$

The vertical variation  $E(z)$  is the solution of the ordinary differential equation of the form

$$\left[ \frac{\partial^2}{\partial z^2} + k_0^2 \epsilon(z) - k_0^2 n_e^2 \right] E(z) = 0 \quad (3)$$

with the boundary condition that  $E(z)$  and  $\partial E(z)/\partial z$  are continuous for all values

of  $z$ .  $n_e$  is the eigen value representing the effective index of the guided mode and  $\epsilon(z)$  is the dielectric constant of the waveguide with no grating. Following the conventional analysis of planar waveguides,  $E(z)$  is normalized such that

$$(k_0 n_e / 2\omega) \int_{-\infty}^{+\infty} E(z) E^*(z) dz = 1 \quad (4)$$

When there is a grating structure on an isotropic single mode planar waveguide, the dielectric constant of Equation (1) must include the variations caused by the grating structure as follows:

$$\epsilon = \epsilon(z) + \Delta\epsilon(x, y, z) \quad (5)$$

and

$$\Delta\epsilon = \Delta\epsilon(z) W(x, y) \epsilon'(x) \quad (6)$$

where  $\epsilon'(x) \Delta\epsilon(z)$  is the deviation of the dielectric constant from  $\epsilon(z)$  of the planar waveguide produced by the grating and  $W(x, y)$  is the window function that defines the presence or absence of the grating,  $W(x, y) = 1$  inside the grating region and  $W(x, y) = 0$  outside the grating region. We have assumed that the deviation of the dielectric constant caused by the grating can be described approximately by the product of two functions  $\Delta\epsilon(z)$  and  $\epsilon'(x)$ . This assumption is strictly valid only for gratings with a rectangular groove profile. In order to demonstrate our analytical method, we shall further assume that

$$\epsilon'(x) = g \cos(Kx + px^2) + \text{higher order terms} \quad (7)$$

where  $g$  is a constant, and the higher order terms of  $\epsilon'$  are negligibly small. The  $\cos(Kx + px^2)$  term describes a fundamental sinusoidal periodic structure with a linear chirp along the  $x$  direction.  $K$  is the fundamental spatial frequency of the grating structures at  $x = 0$  (i.e.,  $K = 2\pi/\Lambda$  at  $x = 0$ ), and  $p$  is the rate at which the spatial frequency  $K$  is chirped. For a quasi-periodic structure with a large chirping rate, the assumption that the higher order terms in Equation (7) could be neglected may not be very accurate and those terms may need to be taken into account. However, the higher order terms of  $\epsilon'$  could be included in our formalism if necessary.

#### B. The Perturbation Formalism for a Single Thin Slab

The diffracted field of any optical guided wave incident on one of the thin grating slabs of Figure 1 can be calculated by a conventional perturbation technique using a Green's function, under two assumptions:

1. The vertical variation (i.e.,  $z$ ) of the incident wave is not disturbed significantly by the grating grooves.
2. Within the interaction length of the grating, the amplitude and the phase of the incident guided wave can be assumed to be known.

The second assumption is generally correct only when the thickness of the thin grating slab is sufficiently thin such that the effect of the reverse scattering from the diffracted beam back into the incident beam can be neglected. In such a perturbation analysis, it is assumed that the total electric field inside the grating slab region can be written in the form:

$$e_t = Ae_{in} + e_d \quad (8)$$

where  $e_{in}$  represents any guided wave incident on the grating and  $e_d$  represents the diffracted field caused by the interaction of the incident wave with the grating structure.  $e_{in}$  satisfies Equation (1).  $Ae_{in}$  is assumed to be much larger than  $e_d$ . The total electric field is to satisfy the scalar wave equation describing the wave propagation within the grating slab:

$$\nabla^2 e_t + k_0^2 [\epsilon(z) + \Delta\epsilon(x,y,z)] e_t = 0 \quad (9)$$

Substituting Equation (8) into Equation (9), we obtain:

$$\nabla^2 e_d + k_0^2 \epsilon(z) e_d = -Ak_0^2 \Delta\epsilon(x,y,z) e_{in} \quad (10)$$

In arriving at Equation (10), the  $k_0^2 \Delta\epsilon e_d$  term and the derivatives of  $A$  have been neglected in the first order approximation. If the excitation of air and substrate modes are also neglected, the incident guided wave  $e_{in}$  and the diffracted guided wave  $e_d$  can be written in the form of Equation (2). Therefore,

$$e_{in} = E(z) \phi_{in}(x,y) \quad (11)$$

$$e_d = E(z) \phi_d(x,y) \quad (12)$$

Substituting Equations (11) and (12) into Equation (10) and utilizing the normalization relation of Equation (4), we obtain a two-dimensional differential equation of the form:

$$[\nabla_t^2 + k_0^2 n_e^2] \phi_d(x,y) = -AC \epsilon'(x) \phi_{in}(x,y) \quad (13a)$$

where  $\nabla_t$  is the horizontal (i.e., x,y) component of the  $\nabla$  operator:

$$\nabla_t = \nabla - \frac{\partial}{\partial z} \hat{z}$$

$\hat{z}$  is a unit vector along z and the constant C in Equation (13a) is defined by

$$C = \left( \frac{k_0^3 n_e}{2\omega\mu} \right) \int_0^\tau \Delta\epsilon(z) E(z) E^*(z) dz \quad (13b)$$

and  $\tau$  is the thickness of the deposited grating groove. The horizontal field distribution of the diffracted field  $\phi_d(x,y)$  can be calculated from Equation (13a) for a known  $\phi_{in}$  by using the appropriate Green's function as following:

$$\phi_d(x,y) = \frac{1}{4\pi} \iint_{\text{over the grating area}} G(x,y; x',y') F(x',y') dx'dy' \quad (14)$$

where  $F(x,y)$  is equal to the right-hand side of Equation (13a). The appropriate Green's function for the differential equation of (13a) is [13]:

$$G(x,y; x',y') = -j H_0^{(2)}(k_0 n_0 R) \quad (15)$$

where

$$R = [(x - x')^2 + (y - y')^2]^{\frac{1}{2}} \quad (16)$$

and  $H_0^{(2)}$  is the Hankel function of the second kind.

We have calculated  $\phi_d(x,y)$  of Equation (14) numerically on a digital computer when  $\phi_{in}(x,y)$  is a planar guided wave with uniform amplitude variation, a planar guided wave with Gaussian amplitude variation, or a cylindrical guided wave. The numerical integrations were performed by expanding the parameter  $R$  represented by Equation (16) in a binomial expansion and taking only the first term of the expansion:

$$\begin{aligned} R &= [(x - x')^2 + (y - y')^2]^{\frac{1}{2}} \\ &\approx (x^2 + y^2)^{\frac{1}{2}} + (x'^2 + y'^2 - 2xx' - 2yy')/2(x^2 + y^2)^{\frac{1}{2}} \end{aligned} \quad (17)$$

In practice, for the structures that we have evaluated, when the thickness of each slab  $\delta$  is less than or equal to one micron and the grating lens had a focal length greater than 10 mm (i.e.,  $y \geq 10$  mm), the term  $y'^2/2(x^2 + y^2)^{\frac{1}{2}}$  in Equation (17) was less than  $5 \times 10^{-5}$ . That term was neglected. Hence, the double integration of Equation (14) was simplified to a single integral over  $x'$ . This single integral was calculated, numerically, by the conventional integration procedure. The integration over  $y'$  was performed analytically. For the grating structures

that we have analyzed, the reduction of the thickness of each slab to less than one micron and the inclusion of the third term of the binomial expansion for  $R$  caused a less than 1% change of the calculated diffraction efficiency. In order to compare our results with the results obtained from the two-dimensional generalized coupled mode analysis, we have only approximated  $\epsilon'(x)$  by the first Fourier component of the dielectric constant perturbation given in Equation (7). However, if necessary, higher Fourier components may be included in the integral of Equation (14) without any further complications.

Figure 2 shows the calculated intensity ( $\phi_d \phi_d^*$ ) of a single grating lens slab on its focal plane when a planar guided wave with uniform amplitude or a planar guided wave with Gaussian distribution of amplitude is incident on it. For both cases, the grating lens has an aperture  $H = 1$  mm, focal length ( $f$ ) = 10 mm with the grating periodicity  $\Lambda$  which varies between  $\Lambda = 13$   $\mu\text{m}$  to  $\Lambda = 2.36$   $\mu\text{m}$  and the width of the grating slab is 1  $\mu\text{m}$ . The diffracted intensity of Figure 2b is obtained when the magnitude of the Gaussian electric field at the edge of the lens slab is  $1/e$  times the magnitude of the electric field at the center of the lens.

### C. The Iterative Perturbation Formalism

Let us consider the first longitudinal slab of the chirped grating lens which is illustrated in Figure 3. For a planar guided wave  $e_{in}^p$  incident on this slab at the angle  $\theta_i$ , the diffracted field  $e_d^{(1)}$  caused by the interaction of the incident wave and the thin grating structure can be calculated using the

perturbation formula of Equation (14):

$$\begin{aligned}
 e_d^{(1)}(x, f) &= E(z) \phi_d^{(1)}(x, f) \\
 &= E(z) / 4\pi \int_0^\delta \int_{-H/2}^{+H/2} C \cdot c'(x) \phi_{in}^p(x', y') [-j\pi H_0^{(2)}(k_0 n_e R_1)] dx' dy'
 \end{aligned}
 \tag{18}$$

where

$$R_1 = [(x - x')^2 + (f - y')^2]^{\frac{1}{2}} \tag{19}$$

The above diffracted field  $e_d^{(1)}(x, f)$  is calculated on a plane ( $p_1$ ) at the distance  $f$  away from the first slab.

Since we have neglected the excitation of the air and substrate modes, the coefficient  $a_1$  which represents the amplitude of the undiffracted planar guided wave after the first section can be calculated from the conservation of the energy between the incident wave  $e_{in}^p$  and the diffracted field  $e_d^{(1)}$  to be:

$$a_1 = \left\{ 1 - \left[ \int_{-\infty}^{+\infty} e_d^{(1)} (e_d^{(1)})^* dx / \int_{-H/2}^{+H/2} e_{in}^p (e_{in}^p)^* dx \right] \right\}^{\frac{1}{2}} \tag{20}$$

It is well known in optics that  $e_d^{(1)}$  consists of a superposition of the fields belonging to various orders of diffraction. Each order of diffraction is a converging or diverging guided wave. The first diffraction order of the diffracted

waves will converge to the point  $[x = -f(K - k_0 n_e \sin \theta_1), y = f]$  where  $f = \frac{k_0 n_e}{2p}$ . Therefore, we assume that the diffracted guided wave emerging from the first slab,  $e_d^{(1)}$  at any distance  $x$  and  $y$ , to be a superposition of cylindrical waves of the form:

$$c_1 H_0^{(1)}(k_0 n_e R_1') + \text{higher order cylindrical guided waves} \quad (21)$$

where

$$R_1' = \{[x + f(K - k_0 n_e \sin \theta_1)]^2 + (y - f)^2\}^{\frac{1}{2}} \quad (22)$$

We have calculated  $c_1$ , which is the amplitude of the first diffraction order cylindrical wave, by separating the total diffracted field on the plane  $P_1$  into two parts, one part due to the  $H_0^{(1)}$  and the second part due to all the other orders of diffraction, as follows.

The diffracted field of  $H_0^{(1)}(k_0 n_e R_1')$  on the plane  $P_1$  is given by the Kirchoff diffraction theory as

$$\psi_c^{(1)}(x, f) = -\frac{1}{4\pi} \int_{-H/2}^{+H/2} G_n(x, f; x', y' = \delta) \phi(x') dx' \quad (23)$$

where  $\phi(x)$  is the boundary value of the cylindrical wave on the plane  $y = \delta$  and  $G_n$  is the normal derivative of the Green's function [13].

On the plane  $P_1$ , we can write:

$$e_d^{(1)}(x, f) = c_1 \psi_c^{(1)}(x, f) + e_s^{(1)} \quad (24)$$

where  $e_s^{(1)}$  represents the diffracted field due to all the higher order cylindrical waves on the plane  $P_1$ .

Now, if  $e_s^{(1)}$  is approximately orthogonal to  $\psi_c^{(1)}$ , then we may obtain  $c_1$  from Equation (24) as

$$c_1 = \int_{-\infty}^{+\infty} e_d^{(1)}(\psi_c^{(1)})^* dx / \int_{-\infty}^{+\infty} \psi_c^{(1)}(\psi_c^{(1)})^* dx \quad (25)$$

From the numerical results of Equations (20) and (25), we have now obtained the amplitudes of the planar guided wave  $A^{(1)}$  and converging cylindrical wave  $B^{(1)}$  emerging from the first slab at  $y = \delta$ , i.e.,  $A^{(1)} = a_1$  and  $B^{(1)} = c_1$ . Both of these waves will be incident on the second slab of the chirped grating lens. The energy scattered into all the higher orders is considered as loss to the incident beam.

Now let us consider the second longitudinal slab of the chirped grating lens as illustrated in Figure 4. For the planar guided wave  $e_{in}^p$  incident on the second slab shown in Figure 4a, the diffracted field  $e_d^{(2)}(x, f + \delta)$  on the plane  $P_2$  can be calculated using Equation (14). However, it can be shown that the diffracted field  $e_d^{(2)}(x, f + \delta)$  on the plane  $P_2$  is related to  $e_d^{(1)}$  on the plane  $P_1$  by the following relation:

$$e_d^{(2)}(x, f + \delta) = \exp(-jk_0 n_e \cos \theta_1 \delta) e_d^{(1)}(x, f) \quad (26)$$

The coefficient  $a_2$  which represents the amplitude of the undiffracted planar guided wave after the second slab is:

$$a_2 = \left\{ 1 - \left[ \int_{-\infty}^{+\infty} e_d^{(2)} (e_d^{(2)})^* dx / \int_{-H/2}^{+H/2} e_{1n}^p (e_{1n}^p)^* dx \right] \right\}^{\frac{1}{2}} = a_1 \quad (27)$$

In Equation (27), we again have neglected the excitation of the air and substrate modes and have assumed the conservation of energy between the incident wave on the second slab and the diffracted field and the undiffracted wave emerging from that slab.

The diffracted field  $e_d^{(2)}$  is again the superposition of the fields due to the converging or diverging cylindrical guided waves coming out of the second slab. These cylindrical waves are of the form:

$$c_2 H_0^{(1)}(k_0 n_e R_2') + \text{higher order cylindrical guided waves} \quad (28)$$

where

$$R_2' = \{ [x + f(k_0 n_e \sin \theta_i)]^2 + (f + \delta - y)^2 \}^{\frac{1}{2}} \quad (29)$$

On the plane  $P_2$ , we can write:

$$e_d^{(2)}(x, f + \delta) = c_2 \psi_c^{(2)} + e_s^{(2)} \quad (30)$$

where  $\psi_c^{(2)}$  is the diffracted field of  $H_0^{(1)}(k_0 n_e R_2')$  on the plane  $P_2$  and  $e_s^{(2)}$  represents the diffracted field due to higher order cylindrical waves.

If  $e_s^{(2)}$  is approximately orthogonal to  $\psi_c^{(2)}$ , then

$$c_2 = \int_{-\infty}^{+\infty} e_d^{(2)} (\psi_c^{(2)})^* dx / \int_{-\infty}^{+\infty} \psi_c^{(2)} (\psi_c^{(2)})^* dx \quad (31)$$

It can be shown that  $\psi_c^{(2)}$ , the diffracted field of  $H_0^{(1)}(k_0 n_e R_2')$  on the plane  $P_2$ , is the same as  $\psi_c^{(1)}$ , the diffracted field of  $H_0^{(1)}(k_0 n_e R_1')$  on the plane  $P_1$ :

$$\psi_c^{(2)}(x, f + \delta) = \psi_c^{(1)}(x, f) \quad (32)$$

Substituting  $e_d^{(2)}$  and  $\psi_c^{(2)}$  in Equation (31) by  $e_d^{(1)} \exp(-jk_0 n_e \cos \theta_1 \delta)$  and  $\psi_c^{(1)}$ , respectively, we obtain:

$$c_2 = c_1 \exp(-jk_0 n_e \cos \theta_1 \delta) \quad (33)$$

The cylindrical wave  $c_1 H_0^{(1)}(k_0 n_e R_1')$ , which has been produced by the interaction of the planar guided wave with the first slab, will also be diffracted by the second slab, shown in Figure 4b. The diffracted field  $e_{dc}^{(2)}$  caused by the interaction of the incident wave  $H_0^{(1)}(k_0 n_e R_1')$  and the second grating slab has been calculated using Equation (14):

$$\begin{aligned} e_{dc}^{(2)}(x, f) &= E(z) \phi_{dc}^{(2)}(x, f) \\ &= E(z)/4\pi \int_{\delta}^{2\delta} \int_{-H/2}^{+H/2} C \varepsilon'(x) H_0^{(1)}(k_0 n_e R_1') [-j H_0^{(2)}(k_0 n_e R_1')] dx' dy' \end{aligned} \quad (34)$$

where  $R_1$  and  $R_1'$  are given by Equations (19) and (22), respectively, and the diffracted field  $e_{dc}^{(2)}$  is calculated on the plane  $P_1$ .

The diffracted waves emerging from the second slab, due to the incident cylindrical wave, can be represented as:

$$b_2 e_{in}^P + \text{higher order planar guided waves} \quad (35)$$

We have calculated the complex amplitude  $b_2$  as follows:

$$b_2 = \int_{-\infty}^{+\infty} e_{dc}^{(2)} (\psi_p^{(2)})^* dx / \int_{-\infty}^{+\infty} \psi_p^{(2)} (\psi_p^{(2)})^* dx \quad (36)$$

where  $\psi_p^{(2)}$  is the diffracted field of  $e_{in}^P$  on the plane  $P_1$ . In obtaining Equation (36), we again have assumed that the diffracted field of the higher order planar waves  $e_{sc}^{(2)}$  are approximately orthogonal to  $\psi_p^{(2)}$ .  $b_2$  in Equation (36) is a complex coefficient which represents the reverse feedback effect of the cylindrical wave into the original plane guided wave caused by the grating structure.

Once again by using the conservation of energy between the incident cylindrical wave  $H_0^{(1)}(k_0 n_e R_1')$  and the diffracted field  $e_{dc}^{(2)}$  and the undiffracted cylindrical wave, we obtain the amplitude coefficient  $d_2'$  of the undiffracted cylindrical wave:

$$d_2' = \left\{ 1 - \left[ \int e_{dc}^{(2)} (e_{dc}^{(2)})^* dx / \int_{-H/2}^{+H/2} H_0^{(1)}(k_0 n_e R_1') [H_0^{(1)}(k_0 n_e R_1')]^* dx \right] \right\}^{\frac{1}{2}} \quad (37)$$

At the output aperture of the second longitudinal slab, two types of cylindrical converging waves exist. One is the cylindrical wave  $c_2 H_0^{(1)}(k_0 n_e R_2')$  which resulted from the interaction of the planar guided wave  $e_{in}^p$  and the second slab of the grating lens, shown in Figure 4a, that converges to the point  $[x = -f(k - k_0 n_e \sin \theta_1), y = f + \delta]$ . The second one is the depleted cylindrical wave  $d_2 H_0^{(1)}(k_0 n_e R_1')$  that converges to the point  $[x = -f(K - k_0 n_e \sin \theta_1), y = f]$ . We shall now show that the cylindrical wave  $d_2 H_0^{(1)}(k_0 n_e R_1')$  can be represented approximately by the cylindrical wave  $d_2 H_0^{(1)}(k_0 n_e R_2')$  as follows.

The diffracted field of  $d_2 H_0^{(1)}(k_0 n_e R_1')$  on the plane  $P_2$ , represented by  $\epsilon_c^{(2)}$ , is calculated using Equation (23) with the appropriate boundary condition. We can write:

$$\epsilon_c^{(2)} = d_2 \psi_c^{(2)} + e_s \quad (38)$$

where  $\psi_c^{(2)}$  is the diffracted field of the cylindrical wave  $H_0^{(1)}(k_0 n_e R_2')$  on the plane  $P_2$ . Now, if  $e_s$  is approximately orthogonal to  $\psi_c^{(2)}$ , we may obtain  $d_2$  from Equation (38):

$$d_2 = \int_{-\infty}^{+\infty} \epsilon_c^{(2)} (\psi_c^{(2)})^* dx / \int_{-\infty}^{+\infty} \psi_c^{(2)} (\psi_c^{(2)})^* dx \quad (39)$$

For the grating structures we analyzed, the absolute value of the coefficient  $d_2$  is of the order of  $(0.9998 \pm 0.0001)$  which means that replacing  $d_2 H_0^{(1)}(k_0 n_e R_1')$  with  $d_2 H_0^{(1)}(k_0 n_e R_2')$  will introduce less than 2% error into the final numerical

results even for 100 slabs of the grating (each 1  $\mu\text{m}$  wide). Since the total width of the grating lenses that are of interest is only a few tens of microns, the above approximation will not cause a large error in our analysis. Now the amplitudes of the planar guided wave  $A^{(2)}$  and converging cylindrical wave  $B^{(2)}$  emerging from the second slab at  $y = 2z$  can be calculated:

$$\begin{aligned} A^{(2)} &= a_2 A^{(1)} + b_2 B^{(1)} \\ B^{(2)} &= c_2 A^{(1)} + d_2 B^{(1)} \end{aligned} \quad (40)$$

The same procedure can be used to calculate the coefficients  $a_3$ ,  $b_3$ ,  $c_3$ , and  $d_3$ , which are the elements of the transfer matrix associated to the third slab. However, it can be shown that ( $a_n = a_1$ ,  $b_n = b_1 \exp(-jk_0 n \cos \theta_1)$ ,  $c_n = c_1 \exp(-jk_0 n \cos \theta_1)$  and  $d_n = d_1$  for  $n = 1, \dots, n$ ). Therefore, once the coefficients  $a_1$ ,  $c_1$ ,  $b_2$  and  $d_2$  are calculated by using the Equations (20), (25), (36), (37) and (39), respectively, all the elements of the transfer matrices associated with each slab would be known.

The knowledge of the elements of the transfer matrix associated with each slab enables us to calculate the complex amplitudes of the two principal guided wave beams after the  $n^{\text{th}}$  slab by a matrix multiplication of the form:

$$\begin{bmatrix} A^{(n)} \\ B^{(n)} \end{bmatrix} = \begin{bmatrix} a_n & b_n \\ c_n & d_n \end{bmatrix} \times \dots \times \begin{bmatrix} a_1 & b_1 \\ c_1 & d_1 \end{bmatrix} \begin{bmatrix} A \\ B \end{bmatrix} \quad (41)$$

where  $A$  is the amplitude of the planar guided wave and  $B$  is the amplitude of the cylindrical converging wave incident on the first slab. However, when the incident

planar guided wave  $e_{in}^p$  is normalized such that

$$\int_{-H/2}^{+H/2} e_{in}^p (e_{in}^p)^* dx = 1$$

then A would be equal to one, i.e.,  $A = 1$  and  $B = 0$ .

For the above initial conditions, the diffraction efficiency  $\eta$  of the grating structure after the  $n^{\text{th}}$  section is given by

$$\eta = \int_{-H/2}^{+H/2} [B^{(n)} H_0^{(1)}(k_0 n_e R_n)] \times [B^{(n)} H_0^{(1)}(k_0 n_e R_n)]^* dx$$

where

$$R_n = \{[x + f(K - k_0 n_e \sin \theta_i)]^2 + (f + (n - 1) \delta - y)^2\}^{1/2}.$$

Strictly speaking, the assumption of the orthogonality of the truncated planar guided waves and cylindrical diverging and converging waves have not been established. However, for the structures that we have analyzed, we have evaluated numerically a few integrals in the form

$$\int_{-\infty}^{+\infty} \psi^* e_s dx \quad \text{and} \quad \int_{-\infty}^{+\infty} \psi \psi^* dx.$$

We have found that

$$\left( \int_{-\infty}^{+\infty} \psi^* e_s / \int_{-\infty}^{+\infty} \psi \psi^* \right) \leq 10^{-5}.$$

Therefore, the quasi-orthogonality assumption made for calculating the matrix elements may not be a bad assumption. Also, in the design of grating lenses,

extreme care is taken to obtain the largest separation between different diffracted orders in order to maximize the signal-to-noise response of the grating lens structure. Hence, the quasi-orthogonality of the diffracted field of different diffraction orders is not far from reality.

### III. NUMERICAL RESULTS

We have used the iterative perturbation analysis to calculate the diffraction efficiency of several linearly chirped grating lenses. In Figure 5, the calculated diffraction efficiency of a chirped grating lens as a function of the interaction length  $d$  of the grating is illustrated. The grating lens structure used in this calculation has a minimum periodicity  $\Lambda_{\min} = 2.06 \mu\text{m}$ , the maximum periodicity  $\Lambda_{\max} = 4.25 \mu\text{m}$ , aperture  $H = 1 \text{ mm}$ , and the focal length  $f = 10 \text{ mm}$ . The diffraction efficiency of the grating lens in Figure 5 is calculated when a planar guided wave with Gaussian distribution of amplitude is incident on the lens and when the magnitude of the Gaussian electric field at the edge of the lens slab is  $1/e$  times the magnitude of the electric field at the center of the lens. When the interaction length  $d$  is approximately  $15 \mu\text{m}$  long, the local  $Q$  factor of the grating structure varies from  $Q_{\min} = 2$  to  $Q_{\max} = 9$ . The coupling coefficient  $K_c$  of the grating lens structure (given by  $K_c = C/k_0^2$  where  $C$  is given by Equation (13b)) is assumed to be  $K_c = 0.1 (\mu\text{m})^{-1}$ . From Figure 5, it is seen that the maximum diffraction efficiency occurs when  $K_c d = \pi/2$ , which is in agreement with the previously reported results [14].

Figures 6a and 6b illustrate the diffraction efficiency of the same grating lens as a function of the angular deviation, i.e.,  $\Delta\theta$ , of the incident guided wave from its Bragg angle as calculated by the generalized coupled mode analysis and iterative perturbation analysis, respectively. The grating lens length  $d$  is assumed to be  $15 \mu\text{m}$ . The efficiency calculated by the generalized coupled mode theory is over-estimated because it ignores the losses of the higher diffraction orders of the medium  $Q$  grating structure.

#### IV. CONCLUSION

We have presented in this paper an iterative perturbation analysis suitable to analyze the diffraction properties of the linearly chirped grating lenses with a medium  $Q$  factor on planar optical waveguides. Using this method, we can obtain data such as the diffraction efficiency and the angular range of the incident wave within which effective diffraction can take place.

However, our iterative perturbation analysis has several limitations. First, we have confined our analysis to the case of a single mode waveguide with negligible radiation loss. Second, we have assumed that the different orders of diffraction due to each grating slab are quasi-orthogonal. This assumption is approximately justifiable only if the grating structure is designed to have well-separated orders of diffraction.

#### ACKNOWLEDGEMENT

This work is supported in part by AFOSR Grant No. 80-0037 with the University of California, San Diego.

# V. REFERENCES

1. Tien, P. K., "Method of Forming Novel Curved Line Gratings and Their Use as Reflectors and Resonators in Integrated Optics," *Opt. Lett.*, 1, 64 (1977).
2. Yao, S. K. and D. E. Thompson, "Chirped Grating Lens for Guided-Wave Optics," *Appl. Phys. Lett.*, 33, 635 (1978).
3. Tien, P. K. and R. J. Capik, "A Thin Film Spectrography for Guided Waves," *Technical Digest, IEEE/OSA Topical Meeting on Integrated and Guided Wave Optics*, Incline Village, Nevada (1980).
4. Hatakoshi, G. and S. Tanaka, "Grating Lenses for Integrated Optics," *Opt. Lett.*, 2, 142 (1978).
5. Tamir, T., "Beam and Waveguide Couplers," *Integrated Optics*, T. Tamir (ed.), Berlin:Springer-Verlag, 1975.
6. Wang, S., "Principles of Distributed Feedback and Distributed Reflector Lasers," *IEEE J. Quantum Electron.*, QE-10, 413 (1974).
7. Katzir, A., A. C. Livanos, J. B. Shellan and A. Yariv, "Chirped Gratings in Integrated Optics," *IEEE J. Quantum Electron.*, QE-13, 269 (1977).
8. Hardy, A and W. Streifer, "Analysis of Waveguided Gaussian Beams Coupled by Misaligned or Curved Gratings," *J. Opt. Soc. Am.*, 69, 1235 (1979).
9. Lin, Z.-Q, S.-T. Zhou, W. S. C. Chang, S. Forouhar and J.-M. Delavaux, "A Generalized Two-Dimensional Coupled Mode Analysis of Curved and Chirped Periodic Structures in Open Dielectric Waveguides," *IEEE Trans. Microwave Theory Tech.*, MTT-29, 881 (1981).
10. Chang, W. S. C., S.-T. Zhou, Z.-Q. Lin, S. Forouhar and J.-M. Delavaux, "Performance of Diffraction Lenses in Planar Optical Waveguides," *3rd Intern. Conf. on Integrated Optics and Fiber Optics, Communications*, San Francisco (1981).

11. Alfernes, R., "Analysis of Optical Propagation in Thick Holographic Gratings," *Appl. Phys.*, 7, 29 (1975).
12. Alfernes, R., "Analysis of Propagation at the Second-Order Bragg Angle of a Thick Holographic Grating," *J. Opt. Soc. Am.*, 66, 353 (1976).
13. Morese, P.M. and Feshbach, H., "Methods of Theoretical Physics," Vol. 1 McGraw-Hill, New York (1953).
14. H. Kogelnik, "Coupled Wave Theory for Thick Hologram Gratings," *Bell Syst. Tech. J.*, 48, 2909 (1969).

## LIST OF FIGURES

1. Illustration of a Linear Chirped Grating Waveguide Lens.
2. The Diffracted Intensity Distribution of a Linear Chirped Grating Lens on its Focal Plane for an Incident Planar Guided Wave.
  - a. Uniform Amplitude Planar Wave.
  - b. Gaussian Amplitude Planar Wave.
3. Illustration of the First Longitudinal Slab of the Grating Lens.
4. Illustration of the Second Longitudinal Slab of the Grating Lens.
  - a. When the Guided Wave Incident on the Slab is a Planar Wave.
  - b. When the Guided Wave Incident on the Slab is a Cylindrical Wave.
5. The Diffraction Efficiency  $\eta$  as a Function of the Interaction Length  $d$  of a Medium Q Linear Chirped Grating Lens.
6. Comparison of the Calculated Diffraction Efficiency of a Medium Q Linear Chirped Grating Lens.
  - a. The result of the coupled mode analysis.
  - b. The result of the iterative perturbation analysis.

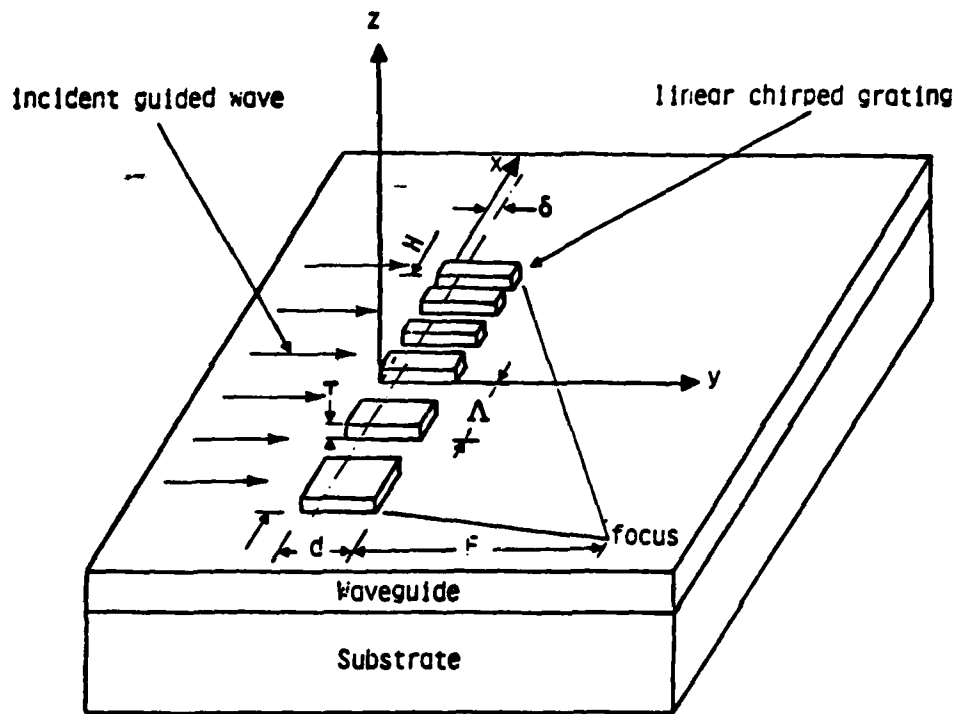


Fig. 1

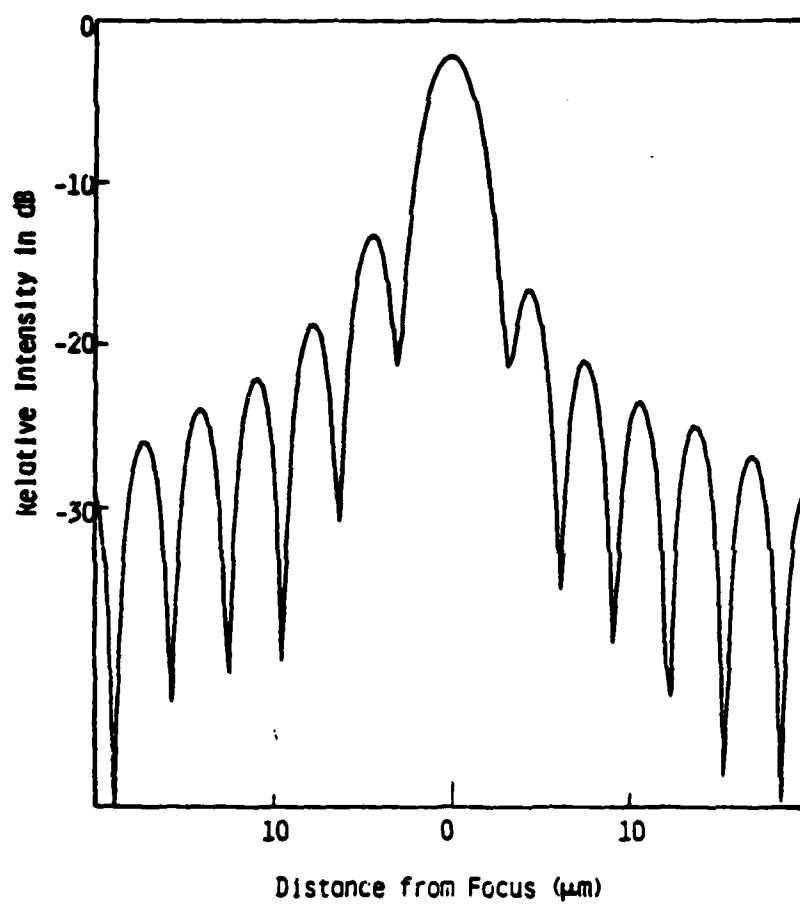


Fig. 2a

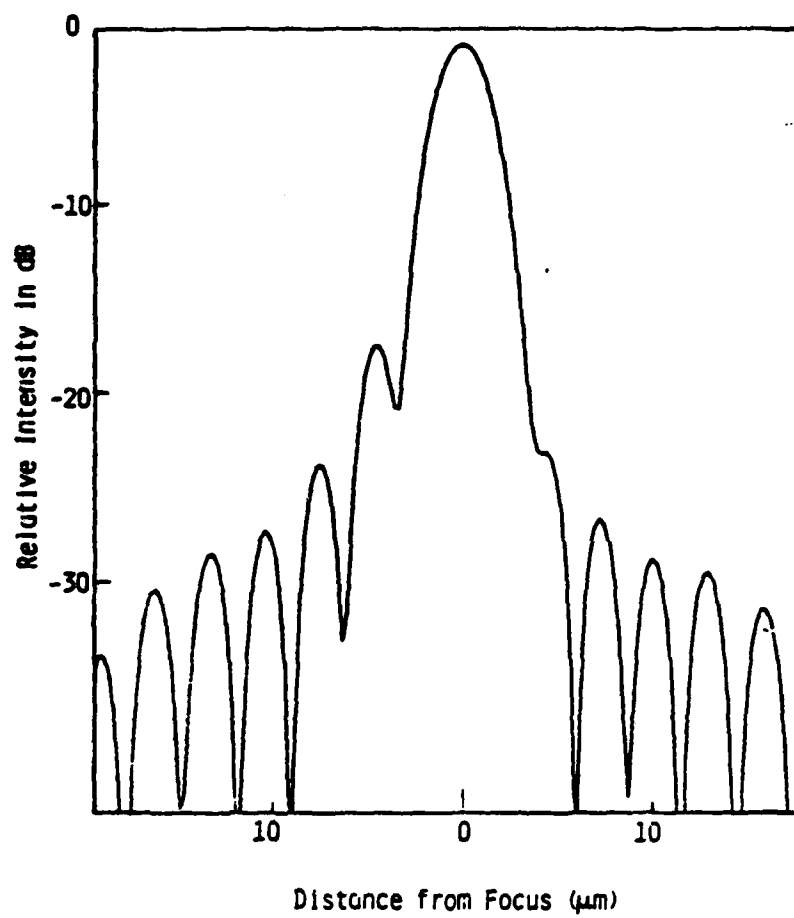


Fig. 2b



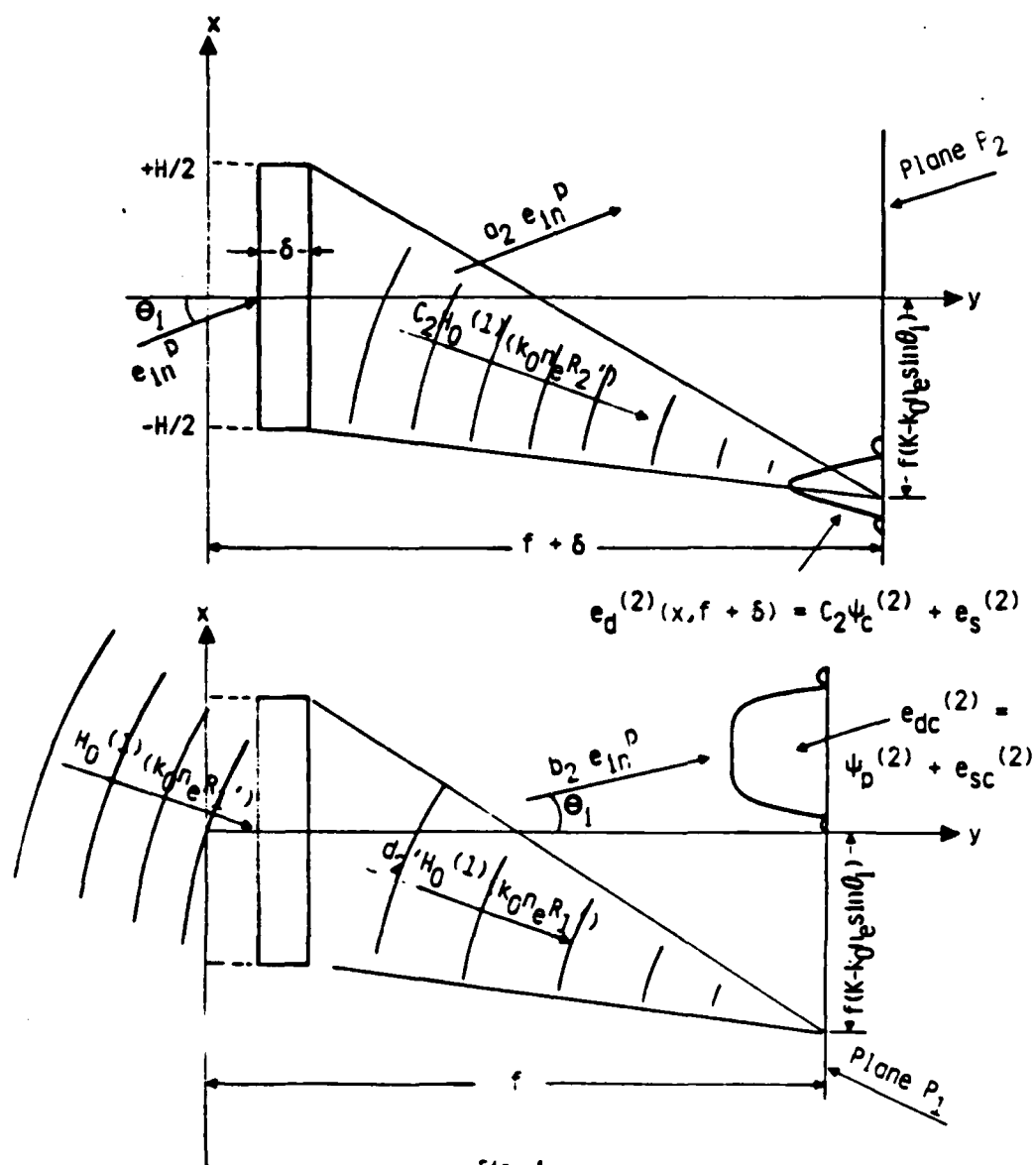


Fig. 4

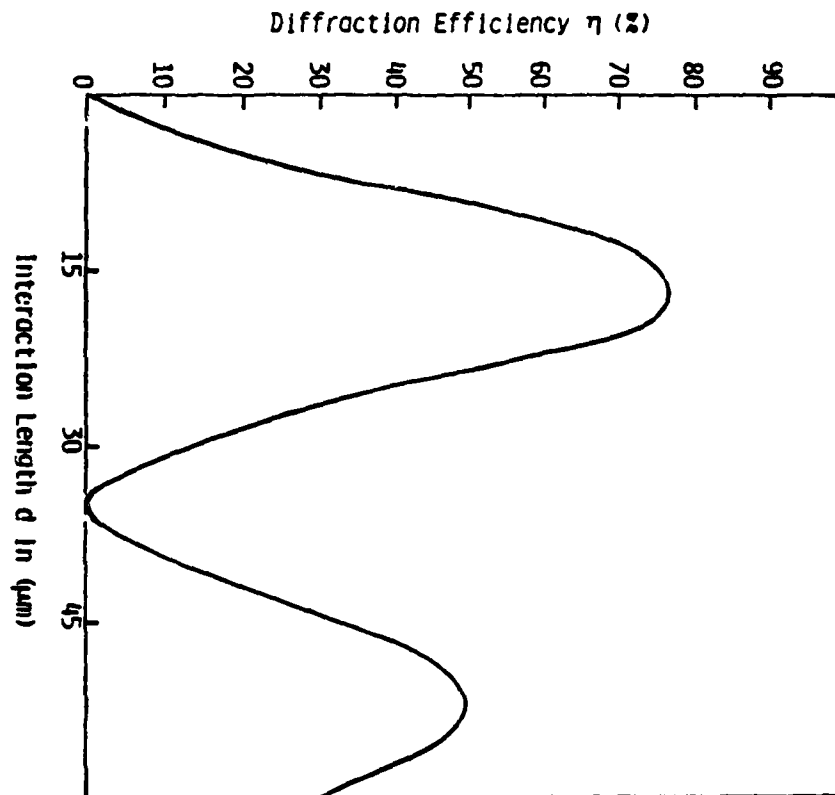


Fig. 5

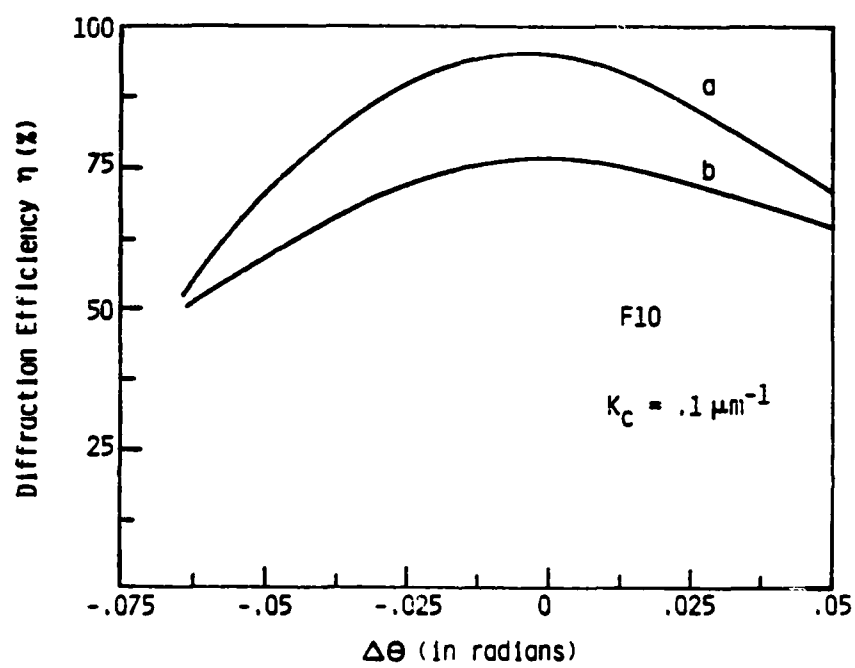


Fig. 6

### CHAPTER III

Performance and Limitations of Chirped Grating Lenses  
on Ti-indiffused  $\text{LiNbO}_3$  Planar Waveguides

by

Siamak Forouhar and William S. C. Chang

University of California, San Diego

Department of Electrical Engineering and Computer Sciences (C-014)

La Jolla, CA 92093

and

Shih-Kay Yao

TRW Technology Research Center

2525 East El Segundo Blvd.

El Segundo, CA 90245

ABSTRACT

Etched and deposited groove chirped grating lenses have been successfully designed, fabricated and evaluated for the first time on Ti-indiffused  $\text{LiNbO}_3$  waveguides. The design procedure, the expected and measured performances, the materials and fabrication processes developed, and the performance limitations imposed by the waveguide parameters and by the fabrication procedures are presented.

## I. INTRODUCTION

There are many potential applications of optical signal processing in planar optical waveguides, such as the rf spectrum analysis, where it is necessary to integrate, focus, collimate, image or Fourier analyze guided wave beams using efficient lenses that have both diffraction-limited performance and low noise. Currently, the most commonly used guided wave lens is a geodesic lens which requires the expensive process of precision grinding of the nonspherical contours for each lens [1].

High efficiency chirped grating lenses on glass waveguides have been initially demonstrated by Yao [2]. Figure 1 illustrates a linearly chirped grating lens. Recently, we have reported the design and experimental evaluation of such lenses on glass waveguides that have a measured total throughput efficiency of 80% with a moderately large angular field of view and diffraction-limited focused spot size [3]. However, for some signal processing applications such as the rf spectrum analyzer, it is necessary to fabricate the grating lenses on Ti-indiffused  $\text{LiNbO}_3$  waveguides. The realization of chirped grating lenses on single mode Ti-indiffused  $\text{LiNbO}_3$  by modulating the surface of the waveguide [4] and on double mode Ti-indiffused  $\text{LiNbO}_3$  by corrugating the surface [5] has been reported recently. However, the performance limitations of grating lenses on such waveguides have never been determined. Serious limitations caused by both the fabrication processes and the availability of materials that have an index higher than  $\text{LiNbO}_3$  can be expected.

We report in this paper the theoretical design of  $\text{LiNbO}_3$  waveguide lenses, the experimental fabrication of these lenses, their measured performance and the limitations that are imposed by the fabrication methods and by the properties of Ti-indiffused  $\text{LiNbO}_3$  waveguides.

## II. THE THEORETICAL GRATING LENS DESIGN

The design of the lenses has been carried out using a generalized coupled mode analysis [6] supplemented by both a perturbation Green's function analysis and an iterative numerical analysis.

The solid curves in Figure 2 show the calculated efficiency  $\eta$  of an  $F$  number = 10 linear chirped grating lens (with  $H = 2$  mm,  $f = 20$  mm,  $\lambda_{\min} = 1.4$   $\mu\text{m}$ , and  $\lambda_{\max} = 2.9$   $\mu\text{m}$ ) as a function of the angular deviation (i.e.,  $\Delta\theta$ ) of the incident guided wave beam from its Bragg angle. The dashed curve in the same figure (using the vertical scale on the right-hand side) shows the calculated focused spot size of this lens. Our calculated results show that high efficiency, nearly diffraction-limited spot size and moderately large  $\Delta\theta$  can be obtained. A better lens performance (i.e., higher efficiency and larger angular field of view) may be obtained using a larger coupling coefficient  $K_c$ . When the perturbation analysis is applicable,  $K_c$  is equal to the change in the effective index in the region inside and outside the grating grooves ( $\Delta n_{\text{eff}}$ ) divided by half of the free-space wavelength  $\lambda_0$ . However, our generalized coupled mode analysis assumes that the power diffracted into the higher order guided wave beams is negligible and that there is very little conversion of guided wave power into the substrate mode. The experimental conditions under which these two assumptions may be valid partially constitute the limitations of the performance of chirped grating lenses.

According to the results of the coupled mode analysis, high efficiency is obtained when the groove length  $d$  is approximately  $\pi/2K_c$ . A larger coupling coefficient implies that a shorter  $d$  may optimize the efficiency. A shorter  $d$  will give a larger angular field of view, defined as the angle within which efficiency  $\eta$  is larger than one-half of its maximum value at  $\Delta\theta = 0$ . Thus, the large

angular field of view shown in Figure 2 is obtained primarily because of the small  $d$  values used. A limitation in the angular field of view (i.e.,  $\Delta\theta$ ) is expected because higher orders of diffraction are expected to occur for the constant periodicity grating at a small  $d$  when the  $Q$  factor ( $Q$  defined as  $2\pi\lambda_0 d/n_{\text{eff}}^2$ ) is significantly less than 10. If the local  $Q$  factor of a chirped grating lens needs to be held equal to 10, the groove length  $d$  can be varied to meet this requirement and the grating groove depth should be adjusted to meet the  $K_c d = \pi/2$  requirement. Our calculated result predicts that a larger angular field of view combined with high efficiency can be expected theoretically for such a lens with controlled  $d$  and  $K_c$  variations.

If only an efficient collimating lens is desired, this can be achieved even with very small  $K_c$  values (i.e., long  $d$ ) provided that a very small angular field of view is acceptable. Theoretically, a parabolic curved chirped grating pattern should be used in this case so that the generalized phase matching conditions can be satisfied much better than with the linear chirped grating lens. Figure 3 illustrates such a curved chirped grating lens.

Ways of achieving large  $K_c$  and small  $d$  without causing significant substrate mode conversion and higher orders of diffraction as well as the verification of the theoretical results are the principal objectives of our experimental investigations. Limitations in materials and fabrications processes may further limit the lens performance.

### III. THE COUPLING COEFFICIENT

The grating grooves can be fabricated by: (a) etching the grooves into the surface; (b) deposition of a material onto the surface; or (c) diffusion of a material into the volume of the optical waveguide. Our theoretical analysis demonstrates that one of the most important parameters in the design of the chirped grating lens is the coupling coefficient. From the perturbation analysis, the coupling coefficient is proportional to the mode index change  $\Delta n_{\text{eff}}$  caused by the grating grooves ( $K_c = 2\Delta n_{\text{eff}}/\lambda_0$ ). The mode index change  $\Delta n$  is defined as the difference in the  $n_{\text{eff}}$  of a planar waveguide without any grating grooves to the  $n_{\text{eff}}$  of a planar waveguide that has been deposited with the same overlay film (or etched to the same depth) as the grating grooves. We have calculated the amount of index perturbation and thus the coupling coefficient caused by each technique for Ti-indiffused LiNbO<sub>3</sub> waveguides and have also investigated the advantage/disadvantage of different fabrication techniques.

The numerical calculation of the effective indices of the modes of graded index optical waveguides, such as Ti-indiffused LiNbO<sub>3</sub>, of arbitrary but known index profile and diffusion parameters has already been reported [7]. The theory of multilayer dielectric waveguides [8] also has been used for the calculation of the effective indices of the modes of graded index waveguides with known index profile and diffusion parameters. A technique similar to the analysis of multilayer dielectric waveguides is used here to calculate the change in the effective index of the mode and the coupling coefficient of the grating structures on Ti-indiffused LiNbO<sub>3</sub> waveguides.

Figure 4 shows the calculated  $K_c$  ( $K_c = 2\Delta n_{\text{eff}}/\lambda_0$ ) that may be obtained by etching the grooves into the surface of Ti-indiffused LiNbO<sub>3</sub> or by depositing

titanium dioxide fingers with a refractive index of 2.63 [9] onto the surface of a Ti-indiffused  $\text{LiNbO}_3$  waveguide. For the case of deposited grooves, the maximum  $\Delta n_{\text{eff}}$  (i.e.,  $K_c$ ) is limited by the titanium dioxide thickness within which only a single mode will exist in a planar waveguide that has an equivalent  $\text{TiO}_2$  layer. For the etched grooves, the maximum  $K_c$  is limited by the cutoff thickness of the Ti-indiffused planar waveguide. The results shown in Figure 4 clearly demonstrate that a larger coupling coefficient is achievable for the waveguides that have a smaller mode depth. The mode depth here is defined as the distance from the surface of the waveguide at which the refractive index of the Ti-indiffused waveguide is equal to the mode index  $n_{\text{eff}}$  of the guided wave. The mode depth defined in this manner has the physical meaning of being the depth at which the evanescent tail of the electric field begins.

The calculation of the mode index change  $\Delta n_{\text{eff}}$  has been carried out assuming that the index profile of the Y-cut Ti-indiffused  $\text{LiNbO}_3$  waveguide can be described by a Gaussian function [7]:

$$n(y) = n_b + \Delta n \exp[-(y/D)^2] \quad (1)$$

where  $n_b$  is the refractive index of the  $\text{LiNbO}_3$  substrate,  $y$  is the depth from the surface of the  $\text{LiNbO}_3$ ,  $\Delta n$  is the index change at the surface and  $D$  is the diffusion depth defined by  $n(D) = n_b + \Delta n/e$ . The index change at the surface  $\Delta n$  is related to the diffusion parameters such as the diffusion time  $t_{\text{diff}}$ , diffusion temperature  $T_{\text{diff}}$ , and thickness of titanium  $\tau_{\text{Ti}}$  [10]:

$$\Delta n = \frac{2}{\sqrt{\tau}} \cdot \frac{\tau_{\text{Ti}}}{D} \cdot \frac{dn_e}{dc} \quad (2)$$

where  $\alpha$  is the number of atoms per unit volume in the deposited film,  $\frac{dn_e}{dc}$  is the index to concentration ratio and the diffusion depth  $D$  is related to the diffusion constant  $D_y$ , in the  $y$  direction, by  $D = 2\sqrt{D_y t_{diff}}$ . For a known  $\Delta n$  and  $D$ , the Ti-indiffused graded index waveguide may be approximated by a stack of step index waveguides. The mode index  $n_{eff}$  then can be calculated from the appropriate transcendental equation of such a multilayer step index structure [11]. When the waveguide structure is perturbed, either by etching or deposition, the same procedure is used to calculate the mode index  $n'_{eff}$  of the perturbed structure. Using the differences of the two indices, we have calculated the  $K_c$ :

$$\begin{aligned} K_c &= 2(n_{eff} - n'_{eff})/\lambda_0 \\ &= 2 \Delta n_{eff}/\lambda_0 \end{aligned} \quad (3)$$

For Figure 4, we have used  $D_y = 4.7 \times 10^{-13}$  cm<sup>2</sup>/sec and  $\Delta n = 0.021$ . However, as shown in Figures 5 and 6, the mode index change of the modified waveguide and therefore the coupling coefficient is strongly dependent on the diffusion constant  $D_y$  and the index profile of the Ti-indiffused LiNbO<sub>3</sub> waveguide. It is known that due to the outdiffusion of LiO<sub>2</sub> during the diffusion of Ti, the index profile cannot be defined accurately as a Gaussian function [12,13]. The values reported for the diffusion constant for Ti into LiNbO<sub>3</sub> in the  $y$  direction also can vary as much as four times [13-15]. Thus, the accurate prediction of the maximum value of  $\Delta n_{eff}$  that can be obtained by different fabrication techniques requires the characterization of the Ti-indiffused LiNbO<sub>3</sub> waveguide as the first step, i.e., the diffusion constant and the diffusion profile should be known for a specific diffusion process.

We have performed experiments on constant periodicity gratings fabricated on Ti-indiffused  $\text{LiNbO}_3$  waveguides in order to verify the perturbation analysis results to determine the coupling coefficient according to a given  $\Delta n_{\text{eff}}$ , i.e.,  $K_c = 2\Delta n_{\text{eff}}/\lambda_0$ . Constant periodicity grating structures have been fabricated by both the deposition of  $\text{TiO}_2$  grating fingers [9] and the etching of the grating grooves. The period  $\Lambda$  of the grating structure is  $2 \mu\text{m}$  with a grating groove length of  $100 \mu\text{m}$ . All the  $n_{\text{eff}}$  measurements have been performed using the prism coupler technique at the He-Ne laser wavelength of  $0.63 \mu\text{m}$ . In order to measure the change in the mode index  $\Delta n_{\text{eff}}$ , the etching of the waveguide or the deposition of  $\text{TiO}_2$  was carried out only over a part of the Ti-indiffused  $\text{LiNbO}_3$  waveguide. The change in the mode index  $n_{\text{eff}}$  of the original waveguide and the  $n'_{\text{eff}}$  of the modified region where the deposition or etching took place was measured by measuring the angle of the laser light on the prism at which the transverse electric guided modes of the waveguide structure have been excited. The absolute accuracy of our measurement system for the mode index values is of the order of  $\pm 0.0003$ . However, the change in the mode index of the modified region with respect to the original Ti-indiffused  $\text{LiNbO}_3$  waveguide could be measured with an accuracy of  $\pm 0.0001$ . The diffraction efficiency of high Q factor constant periodicity gratings can be calculated by the conventional coupled mode analysis [16] to yield:

$$\eta = \sin^2(K_c d) \quad (4)$$

where  $d$  is the length of the grating grooves. Thus, the measurement of  $\eta$  for a given  $d$  is a measure of the coupling coefficient. Figure 7 shows the calculated diffraction efficiency of a  $100 \mu\text{m}$  long constant period grating for different values

of  $K_c$  using Equation (4). In the same figure, the measured efficiencies of the fabricated gratings are illustrated by the dots and the squares. The coupling coefficients for these gratings were calculated using  $K_c = 2\Delta n_{eff}/\lambda_0$  where  $\Delta n_{eff}$  is the respected measured values of index perturbation  $\lambda_0$ . The measured diffraction efficiency is the ratio of the power measured in the diffracted wave to the sum of powers measured in all the orders of diffraction. Since the Q factor of the grating is much larger than 10, only two orders of diffraction exist. Our results have demonstrated good agreement between the theoretical predictions and the experimental measurements of diffraction efficiency. This result implies that  $K_c = 2\Delta n_{eff}/\lambda_0$  may be used to determine  $K_c$  for values up to  $\approx 0.015 (\mu m)^{-1}$ . However, for larger values of  $\Delta n_{eff}$ , the calculated efficiency using  $\eta = \sin^2(2\Delta n_{eff}d/\lambda_0)$  and the measured efficiencies are very much different, shown in Figure 7. This is in contrast to our experimental observations on glass waveguides [17]. This discrepancy is attributed to two factors:

1. The perturbation method of calculating  $K_c$  may not be valid for large values of  $\Delta n_{eff}$  in graded index waveguides.
2. A large mode index change on Ti-indiffused  $LiNbO_3$  introduces substantial substrate mode conversion (discussion in Section V) whereby the substrate mode conversion could reduce the diffraction efficiency

#### IV. FABRICATION AND EVALUATION OF THE GRATING LENSES

Another experimental task was to characterize the Ti-indiffused waveguides fabricated in our laboratory and to measure the maximum mode index perturbation feasible on such single mode Ti-indiffused waveguides. All optical waveguides were fabricated on Y-cut acoustic-grade  $\text{LiNbO}_3$  substrates. The Ti film was deposited by electron beam evaporation at  $2.0 \times 10^{-7}$  Torr pressure. The thickness of the evaporated Ti film was controlled to be  $165 \pm 5 \text{ \AA}$ . We have observed that all waveguides having a Ti thickness larger than  $190 \text{ \AA}$  are multimode. The diffusion of Ti in  $\text{LiNbO}_3$  was performed in an  $\text{Al}_2\text{O}_3$  tube placed in a temperature-controlled furnace ( $\pm 1^\circ\text{C}$ ) which was preheated to  $1000^\circ\text{C}$ . The diffusion took place under wet oxygen, with an oxygen flow rate of 500 cc/min. The oxygen gas had been passed through a temperature-controlled water bubbler (i.e., wet oxygen) to compensate for the outdiffusion of Li [18]. Waveguides fabricated in this manner had typically an attenuation of 1 dB/cm or less. All the attenuation measurements also were performed using prism couplers. The Ti-indiffused  $\text{LiNbO}_3$  waveguides then were covered partly by a  $\text{TiO}_2$  deposited film or etched in order to measure the mode index change  $\Delta n_{\text{eff}}$ . Figure 8 shows the measured values of the mode index change as a function of the  $\text{TiO}_2$  deposited film thickness for two different diffusion processes. In the same figure, the calculated mode index change as a function of  $\text{TiO}_2$  thickness is plotted for comparison.

All the Ti-indiffused  $\text{LiNbO}_3$  waveguides used for the experimental data illustrated in Figure 8 were made by the evaporation of  $165 \text{ \AA}$  of Ti film followed by the diffusion of Ti into  $\text{LiNbO}_3$  at  $1000^\circ\text{C}$  for 1 hour. The triangles represent the measured mode index change introduced by different thicknesses of the  $\text{TiO}_2$  film when the temperature of the water in the bubbler was kept at  $24^\circ\text{C}$ .

during the diffusion of the Ti film. The large dots represent the same result when the water was kept at 95°C. We have observed experimentally that, for the same thickness of  $\text{TiO}_2$  film, the mode index change  $\Delta n_{\text{eff}}$  can vary as much as five times depending on the temperature of the water inside the bubbler which was used to compensate for the outdiffusion of the  $\text{LiO}_2$ . Figure 9 illustrates the measured mode index change as a function of the etched depth of Ti-indiffused  $\text{LiNbO}_3$  waveguides. These results were obtained for an original waveguide that had 165 Å of Ti deposited on top of the  $\text{LiNbO}_3$  and diffused for 150 minutes at 1000°C when the temperature of the water was kept at 95°C. From the results demonstrated in Figures 8 and 9, we have concluded that a relatively large  $\Delta n_{\text{eff}}$  can be obtained at small thicknesses only if (a) the grating grooves are fabricated by deposition of a high index material such as  $\text{TiO}_2$  and (b) the original waveguides are fabricated under high water vapor pressure during the diffusion process. Using such a process, the behavior of our fabricated single mode Ti-indiffused waveguides can best be described by assuming a Gaussian profile for the index and a diffusion constant  $D_y$  equal to  $3.5 \times 10^{-13} \text{ cm}^2/\text{sec}$ .

Using the forgoing process of waveguide fabrication, several chirped grating lenses were fabricated and evaluated on Ti-indiffused waveguides. The results are listed in Table 1. All our grating lenses were fabricated by replication of the Cr mask pattern onto a  $\text{LiNbO}_3$  waveguide by the conformable optical contact printing method. The Cr masks were made by electron beam lithography at the NSF National Research and Resource Facility for Submicron Structures at Cornell University. For etched grooves, the resist pattern was post-baked at 140°C for two hours and etched by the reactive ion beam etching technique using freon  $\text{C}_3\text{F}_8$  gas. The deposited  $\text{TiO}_2$  grating fingers were obtained by first evaporation of a Ti layer onto the sample that already had the desired resist pattern. Samples

with the desired Ti patterns remaining after lift-off were then oxidized at 450°C in 2000 cc/min dry oxygen to obtain the  $\text{TiO}_2$  chirped grating lens. The throughput efficiencies of the lenses listed in Table 1 were obtained by taking the ratio of the optical power (detected in the focused diffracted guided wave beam) to the power measured in the transmitted optical beam when the incident beam was moved transversely to bypass the lens. The substrate energy conversion due to the lens was determined by subtracting from one the ratio of the sum of the guided wave powers (in all orders of diffraction) to the power transmitted bypassing the lens. The angular field of view of the grating lens was obtained experimentally by measuring the diffraction efficiency as a function of the angle of incidence of the guided wave beam. The angular field of view is the angular range within which the diffraction efficiency is larger than 50% of the maximum diffraction efficiency.

Our experimental results demonstrate that for a large F number, i.e., slow chirping rate, high throughput efficiency can be obtained if: (a) the coupling coefficient  $K_c$  is controlled to maximize the efficiency  $\eta$  for a given groove length  $d$  and (b) the diffraction into higher orders and mode conversion into the substrate mode is negligible. Throughput efficiency of 85% for  $\text{TiO}_2$  deposited grooves 450 Å thick and 80% for etched grooves 1700 Å deep was measured for an F28 chirped grating lens on Ti-indiffused  $\text{LiNbO}_3$ . However, the etched grating lens required much deeper grooves as compared to the deposited grating lens, which resulted in the leakage of the optical guided wave into the substrate. The angular field of view of the F28,  $d = 200 \mu\text{m}$ , lens was limited to  $\sim 1.5^\circ$  primarily because of the long groove length of the structure. Both our theoretical and experimental results demonstrate a drop in the diffraction efficiency of small F number lenses for long grooves and small  $K_c$  even if  $K_c d$  is approximately equal to

$\pi/2$ . This is because, for small F number grating lenses, a significant portion of the input beam will not be at the Bragg angle due to the fast chirping in the periodicity of the grating. In other words, only within a small range of  $\Lambda$  along the lens will the Bragg diffraction condition approximately be satisfied. When the Bragg condition is not fulfilled, the interaction of the grating with the input beam weakens and thereby the diffraction efficiency drops. The calculated efficiency of F = 7 chirped grating lenses by the generalized coupled mode analysis is 24% which is in good agreement with our experimentally measured efficiency. However, we anticipate the the fabrication tolerance of small  $\Lambda$  may cause some degradation on the diffracted intensity pattern of the F = 7 lens.

The experimental results also demonstrate that the relatively larger angular field of view ( $\Delta\theta = 6^\circ$ ) can be obtained by utilizing a shorter length d for the grating lens. However, due to the limitation of the coupling coefficient, the diffraction efficiency would be significantly reduced. We also have observed that the higher orders of diffraction could contain a significant amount of power if the Q factor of the grating lens is smaller than 10.

TABLE 1. EXPERIMENTAL RESULTS OF GRATING LENSES  
ON T1-INDIFFUSED  $\text{LiNbO}_3$  WAVEGUIDES

Lens Specifications					Results		Comments	
$\lambda_{\min}$ ( $\mu\text{m}$ )	$\lambda_{\max}$ ( $\mu\text{m}$ )	d ( $\mu\text{m}$ )	F (mm)	A (mm)	$\eta$ %	$\Delta\theta^\circ$	Higher Diffraction Orders	Substrate Energy Conversion
1.73	3.45	150	12	1.	60	$\approx 2^\circ$	negligible	negligible
4.0	7.76	200	28	1.	85	$\approx 1.5^\circ$	exists but contains little energy	negligible
*4.0	7.76	200	28	1.	80	$\approx 1.5^\circ$	exists but contains little energy	$\approx 10\%$
4.0	7.76	50	28	1.	16	$\approx 6^\circ$	$\approx 10\%$	$\approx 30\%$
1.1	3	150	7	1.	25	$< 1^\circ$	negligible	$< 10\%$
+1.73	3.45	150	12	1.	70	$\approx 1.5^\circ$	negligible	negligible

\* Etched grooves  
+ Two mode waveguide

$\lambda_{\min}$  Minimum Periodicity  
 $\lambda_{\max}$  Maximum Periodicity  
 d Interaction Length  
 F Focal Length  
 A Aperture  
 $\eta$  Throughput Efficiency  
 $\Delta\theta$  Field of View

#### V. LIMITATIONS OF THE GRATING LENS PERFORMANCE ON Ti-INDIFFUSED LiNbO<sub>3</sub>

Even though chirped grating lenses with high throughput efficiency ( $\eta = 90\%$ ) and large angular field of view ( $\Delta\theta = 6^\circ$ ) have been fabricated on glass optical waveguides, the performance of the grating lenses are very much limited when fabricated on Ti-indiffused LiNbO<sub>3</sub> waveguides due to the inherent differences between Ti-indiffused LiNbO<sub>3</sub> and glass waveguides. The closeness of the mode index of Ti-indiffused LiNbO<sub>3</sub> to its substrate index is the major difference that limits the grating lens performance. There are two reasons for making this conclusion.

- (1) When the mode index is very close to the substrate index, any abrupt change in the structure of the optical waveguide, e.g., due to the presence of grating grooves, will result in the conversion of the guided wave energy into the substrate. We have investigated this source of loss both experimentally and theoretically. Figure 10 shows the calculated percentage of the guided optical energy converted to the substrate as a function of the TiO<sub>2</sub> film thickness when a guided wave mode in the section of the Ti-indiffused waveguide without any TiO<sub>2</sub> film is incident normally on another section of the waveguide that has a TiO<sub>2</sub> overlay film. (We call it the TiO<sub>2</sub> pad.) The edge of the film is assumed to be abrupt in the depth direction. The theoretical results were obtained using a procedure similar to that used by Marcuse [19] to calculate the radiation losses of a step discontinuity in an optical waveguide. The large dots in Figure 10 represent the measured substrate energy conversion of constant periodicity ( $\Lambda = 3 \mu\text{m}$ ,  $d = 100 \mu\text{m}$ ) grating

structures fabricated by deposited  $\text{TiO}_2$  films of different thicknesses. The solid squares represent the same results for  $\text{TiO}_2$  pads. Our experimental results demonstrate that for waveguides with  $n_{\text{eff}} - n_{\text{sub}} \approx 0.004$ , a mode index change of the order or larger than 0.004 will result in a severe conversion of the guided mode energy into the substrate mode. We have also measured the amount of substrate mode conversion due to the etched grooves. It is evident that the substrate energy conversion for etched grooves is even more severe than for deposited grooves. In contrast, we have not observed such a substrate mode conversion effect in glass waveguide or in ion-exchanged  $\text{LiNbO}_3$  waveguides.

The conversion of guided energy into the substrate reduces the throughput efficiency of the chirped grating lens and causes additional noise which should be avoided in any integrated optical system. The maximum  $\Delta n_{\text{eff}}$  achievable for our single mode Ti-indiffused  $\text{LiNbO}_3$  waveguide without substrate mode conversion, is approximately  $\approx 0.005$ . Therefore, for efficient interaction between the incident wave and the grating, the groove length  $d$  should be  $\approx 100 \mu\text{m}$ . For a  $100 \mu\text{m}$  length and an average periodicity of  $4 \mu\text{m}$ , the angular field of view is limited to  $1.5^\circ$ . However, a larger angular field of view is achievable at the expense of lower efficiency if a shorter groove length is used.

- (2) The small difference between the mode index and the substrate index also may cause energy leakage to the substrate modes by the grating lens, even for the small index change  $\Delta n_{\text{eff}}$ . First consider the

momentum (K-vector) diagram of a constant periodicity grating on an optical waveguide as shown in Figure 11. The solid triangle represents the phase-matched scattering from one guided wave beam to another guided wave beam by the grating vector  $K$ . The relationship between  $K$  and the Bragg angle  $\theta_B$  is given by the well-known Bragg condition. If the incidence optical beam is offset from the Bragg angle by the amount  $\Delta$ , the K-vector phase-matching condition may be illustrated by the dashed triangle (Figure 11). Substantial scattering of the guided wave energy into the substrate may occur. Figure 12 shows the measured substrate mode conversion for a constant periodicity grating ( $\Lambda = 3 \mu\text{m}$ ,  $d = 100 \mu\text{m}$ ) as the angle of the incident guided wave beam deviates from the Bragg angle  $\theta_B$ . The mode index  $n_{\text{eff}}$  of the Ti-indiffused  $\text{LiNbO}_3$  waveguide used for this experiment was  $\sim 2.2043 \pm .0003$ . The Bragg angle  $\theta_B = \sin^{-1}(\lambda_0/2n_{\text{eff}})$  was calculated to be .048 radians. Our experimental results demonstrate that the substrate energy leakage starts even before the momentum condition of Figure 11 is completely satisfied.

Now consider a chirped grating structure as a summation of transverse sections of gratings that have a constant periodicity  $\Lambda$  within each narrow section. The phase-matching condition for efficient volume interaction between the incident wave and the diffracted wave is satisfied for a given transverse section when the periodicity  $\Lambda$  of the grating grooves satisfies the Bragg condition  $K = 2n_{\text{eff}}k_0 \sin \theta_B$  where  $K = 2\pi/\Lambda$  and  $k_0 = 2\pi/\lambda_0$ . It has been pointed out by Yao [20] that if the projection of the K vector on

the direction of the incident beam  $K\sin\theta_g$  is large enough such that  $K\sin\theta_g \geq (n_{\text{eff}} - n_{\text{sub}})k_0$ , the incident guided wave also will be coupled to the substrate modes that have a propagation wave number equal to or smaller than  $k_0 n_{\text{sub}}$ . This condition implies that the angular field of view and the efficiency of the small F number lenses may be limited due to the coupling into the substrate modes even for small  $\Delta n_{\text{eff}}$ . However, we expect this effect will be dependent on the grating structure parameters ( $d, \Lambda, K_c$ ) and on the optical beam size. Substrate energy conversion has never been observed in glass waveguides.

### CONCLUSION

Etched and deposited groove chirped grating lenses have been successfully designed, fabricated and evaluated for the first time on Ti-indiffused  $\text{LiNbO}_3$  waveguides. A throughput efficiency of 85% for  $\text{TiO}_2$  deposited grooves and 80% for etched grooves has been measured for some lenses. However, it has been determined that due to the properties of Ti-indiffused  $\text{LiNbO}_3$  waveguides, it is difficult to combine high efficiency with large angular field of view on such waveguides. The limitations are caused primarily by the closeness of the mode index to the substrate index of Ti-indiffused  $\text{LiNbO}_3$  waveguides. The largest coupling coefficient that we have measured without any substrate mode conversion is  $\approx 0.015 (\mu\text{m})^{-1}$  and it is obtained with deposited grooves. Our results demonstrate that the major source of the substrate mode conversion is due to the abrupt change in the structure of the waveguide caused by the grating grooves. This problem may be alleviated if the grooves are fabricated by ion-exchange in benzoic acid [21] instead of etching or deposition. Due to the diffusion nature of the ion-exchange process, the index change caused by the grooves is more gradual as compared to etched or deposited fingers. However, the lateral diffusion of ion-exchange may put a limit on the effectiveness of that process for small periodicity structures. Alternative waveguides with a larger  $n_{\text{eff}}$  also may be used to obtain chirped grating lenses [22,23].

ACKNOWLEDGEMENTS

This work is supported by AFOSR Grant No. 80-0037 with the University of California, San Diego and by Air Force Avionics Laboratory Contract No. F33615-82-C-1751 with TRW Technology Research Center and the University of California, San Diego. The authors wish to thank Jean-Marc Delavaux and the NSF National Research and Resource Facility for Submicron Structures at Cornell University for making the chirped grating masks using Electron Beam lithography.

# REFERENCES

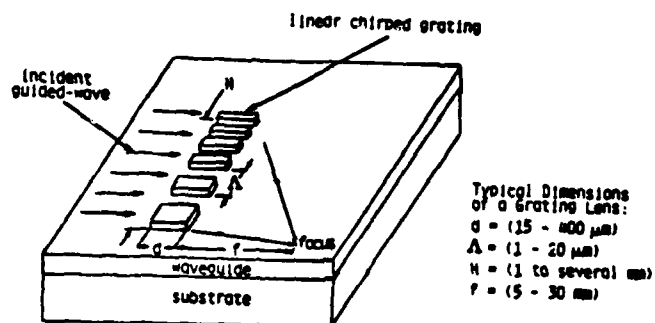
1. Chen, B., I. R. Ranganath, T. R. Joseph and J. Y. Lee, "Progress on the Development of Integrated Optic Spectrum Analyzer," *Topical Meeting on Integrated and Guided Wave Optics*, Incline Village, Nevada (1980).
2. Yao, S. K. and D. E. Thompson, "Chirped Grating Lens for Guided Wave Optics," *Appl. Phys. Lett.*, **33**, 635 (1978).
3. Delavaux, J.-M., S. Forouhar, W. S. C. Chang and R.-X. Lu, "Experimental Fabrication and Evaluation of Diffraction Grating Lenses in Planar Optical Waveguides," presented at IEEE/OSA CLEO, Phoenix, AZ (1982).
4. Chang, W. S. C., S. Forouhar, J.-M. Delavaux, C. Warren and R.-X. Lu, "Chirped Grating Lenses in Ti-indiffused LiNbO<sub>3</sub> Waveguides," *Proceedings of Max Born Centenary Conference (Optics 82, ECOSA 82) SPIE*, **369**, 581 (1982) Edinburgh, Scotland.
5. Stockman, M. and W. Beinvogl, "Planar Bragg Grating Lenses in LiNbO<sub>3</sub> Fabricated by CHF<sub>3</sub> Reactive Ion Etching," to be published in *Wave Electronics* (1983).
6. Lin, Z.-Q., S.-T. Zhou, W. S. C. Chang, S. Forouhar and J.-M. Delavaux, "A Generalized Two-dimensional Coupled Mode Analysis of Curved and Chirped Periodic Structures in Open Dielectric Waveguides," *IEEE Trans. Microwave Theory Tech.*, **MTT-29**, 881 (1981).
7. Hocker, G. B. and W. K. Burns, "Modes in Diffused Optical Waveguides of Arbitrary Index Profile," *IEEE J. Quantum Electron.*, **QE-11**, 270 (1975).
8. Harris, J. H., R. Shubert and J. N. Polky, "Beam Coupling to Films," *J. Opt. Soc. Amer.*, **60**, 1007 (1970).
9. Forouhar, S., C. Warren, R.-X. Lu and W. S. C. Chang, "Techniques for Fabricating High Index Overlay Films on LiNbO<sub>3</sub>," *SPIE Techn. Symp.*, Arlington, VA (1983).

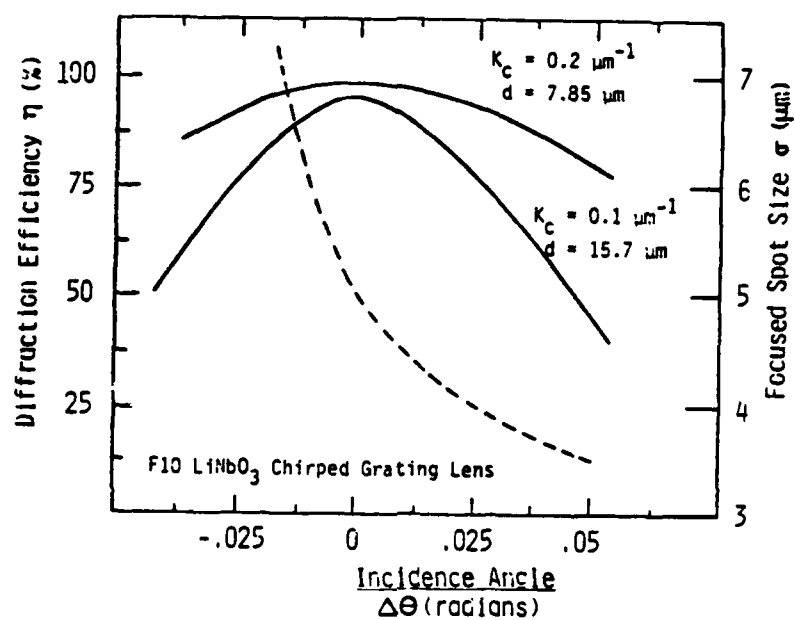
10. Schmit, R. V. and I. P. Kaminov, "Metal Diffused Optical Waveguides in  $\text{LiNbO}_3$ ," *Appl. Phys. Lett.*, 25, 458 (1974).
11. Walpita, L. M., "Langmuir Films in Integrated Optics," Ph.D. Thesis, University College, Longon, England (1977).
12. Naith, H., M. Nunoshita and T. Nakayama, "Mode Control of Ti-indiffused  $\text{LiNbO}_3$  Slab Optical Waveguide," *Appl. Opt.*, 16, 2546 (1977).
13. Griffiths, G. J., "Optical Waveguide Fabrication Techniques," Ph.D. Thesis, University of Queensland, Australia (1981).
14. Burns, W. K., P. H. Keline, E. J. West and L. E. Plew, "Ti-indiffused  $\text{LiNbO}_3$  Planar and Channel Waveguides," *J. Appl. Phys.*, 50, 6175 (1979).
15. Fukuma, N. J. and H. Iwasaki, "Optical Properties in Ti- $\text{LiNbO}_3$  Strip Waveguides," *J. Appl. Phys.*, 49, 3693 (1978).
16. Kogelnik, H., "Coupled Wave Theory for Thick Hologram Gratings," *Bell Syst. Tech. J.*, 48, 2909 (1969).
17. "Fresnel Lenses and Beam Control in Optical Waveguides," Annual Report AFOSR/NE 480-0037.
18. Jackel, J. L., V. Ramaswamy and S. P. Lyman, "Elimination of Outdiffusion Surface Guiding in Ti-indiffused  $\text{LiNbO}_3$ ," *Appl. Phys. Lett.*, 38, 509 (1981).
19. Marcuse, D., "Radiation Losses of Tapered Dielectric Slab Waveguides," *Bell Syst. Tech. J.*, 49, 1273 (1970).
20. Yao, S. K., "Limitations of Holographic Grating Lenses," *SPIE Integrated Optics*, 269, 45 (1981).
21. Jackel, J. L., C. E. Rice and J. J. Vaselka, Jr., "Proton Exchange for High Index Waveguides in  $\text{LiNbO}_3$ ," *IEEE/OSA Optical Meeting in Integrated and Guided Wave Optics*, Pacific Grove, CA (1982).

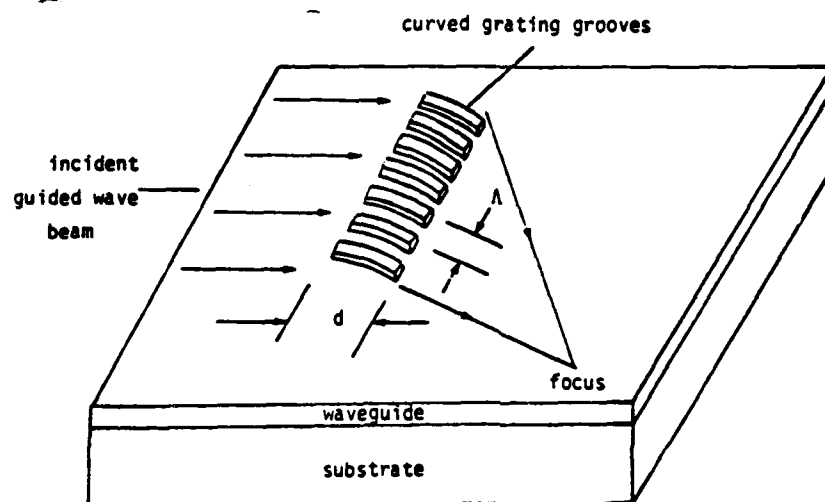
22. Warren, C., S. Forouhar, W. S. C. Chang and S. K. Yao, "Double Ion Exchange Chirped Grating Lens in  $\text{LiNbO}_3$  Waveguides," to be published in *Appl. Phys. Lett.*, September (1982).
23. Forouhar, S., R.-X. Lu, W. S. C. Chang, R. L. Davis and S. K. Yao, "Chirped Grating Lenses on  $\text{Nb}_2\text{O}_5$  Transition Waveguides," to be published in *Appl. Optics*, October (1983).

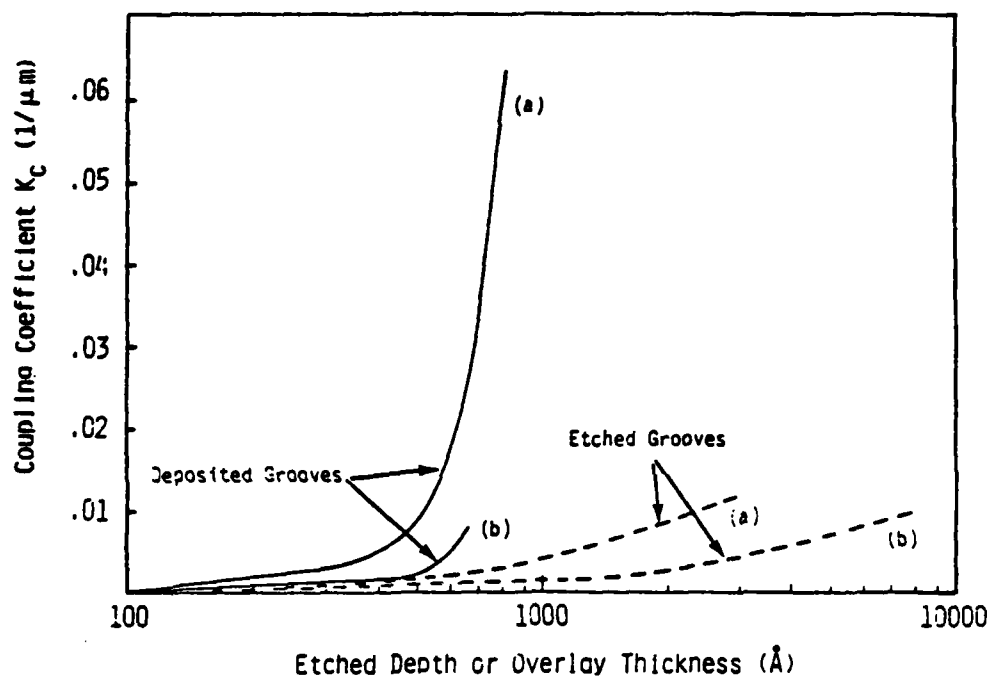
# LIST OF FIGURES AND TABLES

- Figure 1: Illustration of a Linear Chirped Grating Waveguide Lens.
- Figure 2: Focused Spot Size and Diffraction Efficiency as a Function of the Angular Deviation of the Incident Wave from Its Bragg Angle.
- Figure 3: Illustration of a Curved Chirped Grating Waveguide Lens.
- Figure 4: Comparison of  $K_c$  for Etched  $\text{LiNbO}_3$  and Deposited  $\text{TiO}_2$  Fingers on  $\text{LiNbO}_3$  Waveguides.
- Figure 5: Variation of the Mode Index Change as a Function of  $\text{TiO}_2$  Deposited Overlay Films for Different Diffusion Constants.
- Figure 6: Variation of the Mode Index of Ti-indiffused Waveguides as a Function of  $\text{TiO}_2$  Deposited Overlay Films for Different Diffusion Profiles.
- Figure 7: Diffraction Efficiency of a 100  $\mu\text{m}$  Long Constant Periodicity Grating as a Function of the Coupling Coefficient.
- Figure 8: Mode Index Change Versus Thickness of a  $\text{TiO}_2$  Deposited Overlay.
- Figure 9: Mode Index Change Versus Etched Depth of a Ti- $\text{LiNbO}_3$  Waveguide.
- Table 1: Experimental Results of Grating Lenses on Ti-indiffused  $\text{LiNbO}_3$  Waveguides.
- Figure 10: Substrate Energy Conversion versus Thickness of  $\text{TiO}_2$  Deposited Films.
- Figure 11: Momentum Vector Diagram of a Constant Periodicity Grating.
- Figure 12: Substrate Energy Conversion versus Angular Deviation of the Incident Wave from its Bragg Angle.

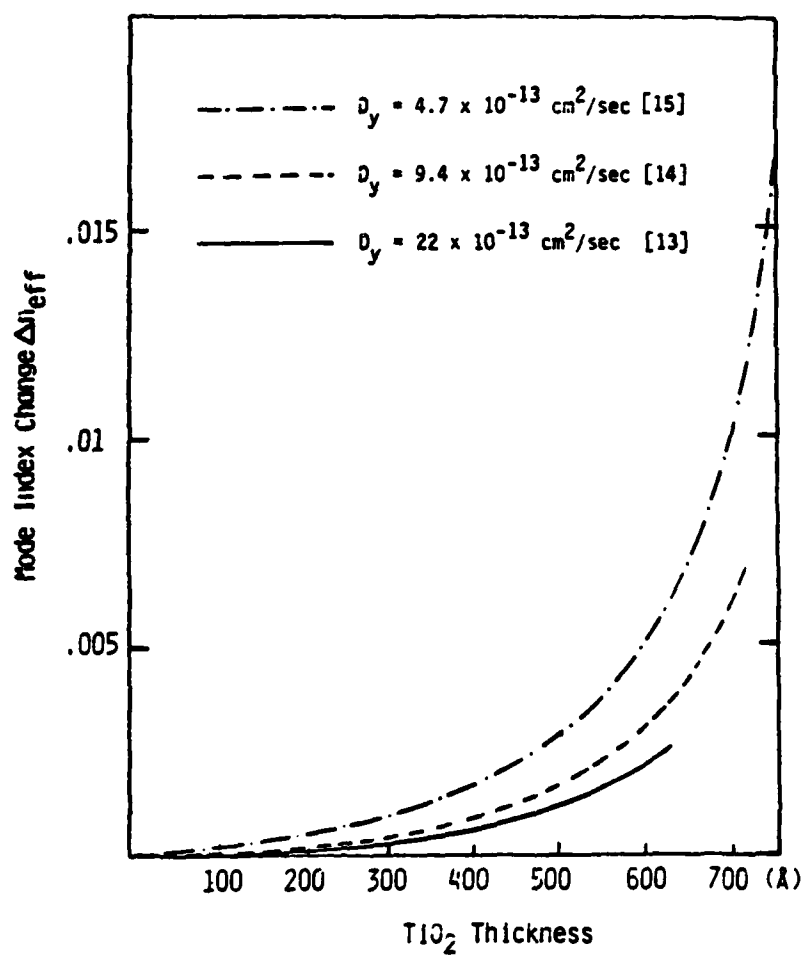


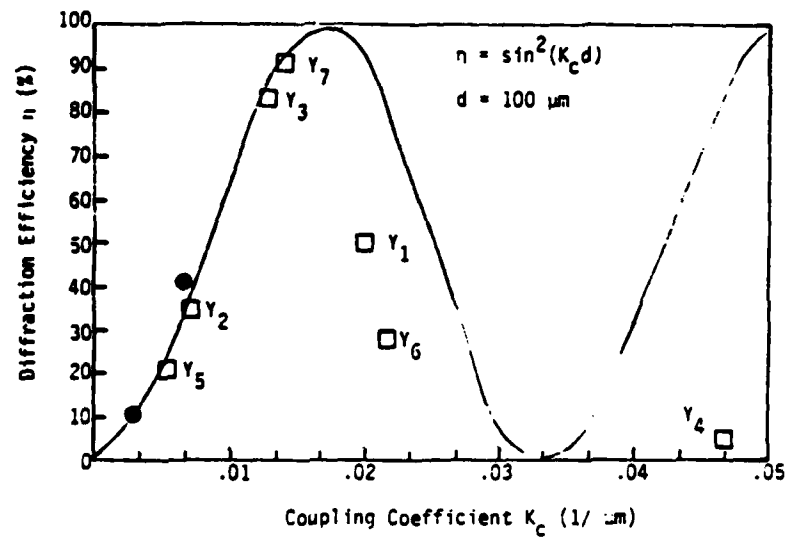




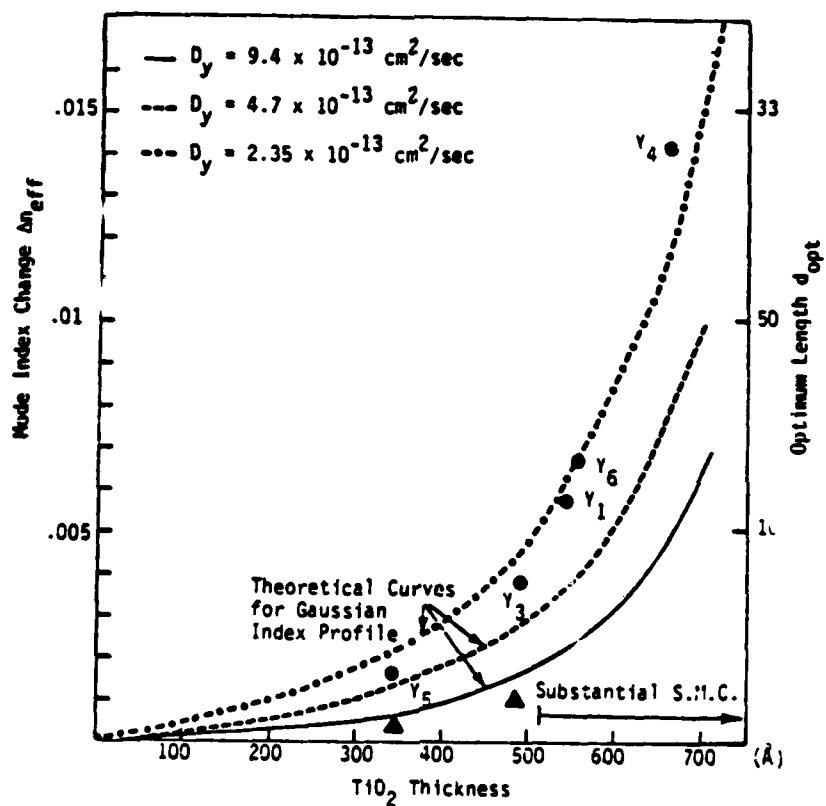


- (a) The effective mode depth of the waveguide is  $1\ \mu\text{m}$ .  
 (b) The effective mode depth of the waveguide is  $2\ \mu\text{m}$ .



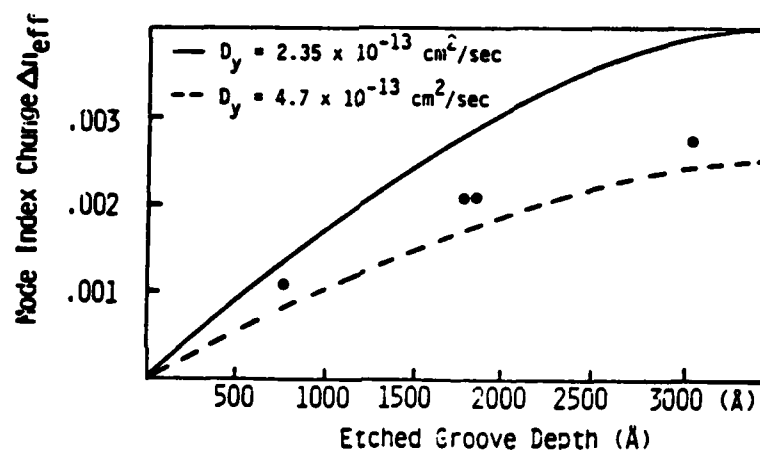


- Experimental results for deposited  $\text{TiO}_2$  grooves.
- Experimental results for etched grooves.

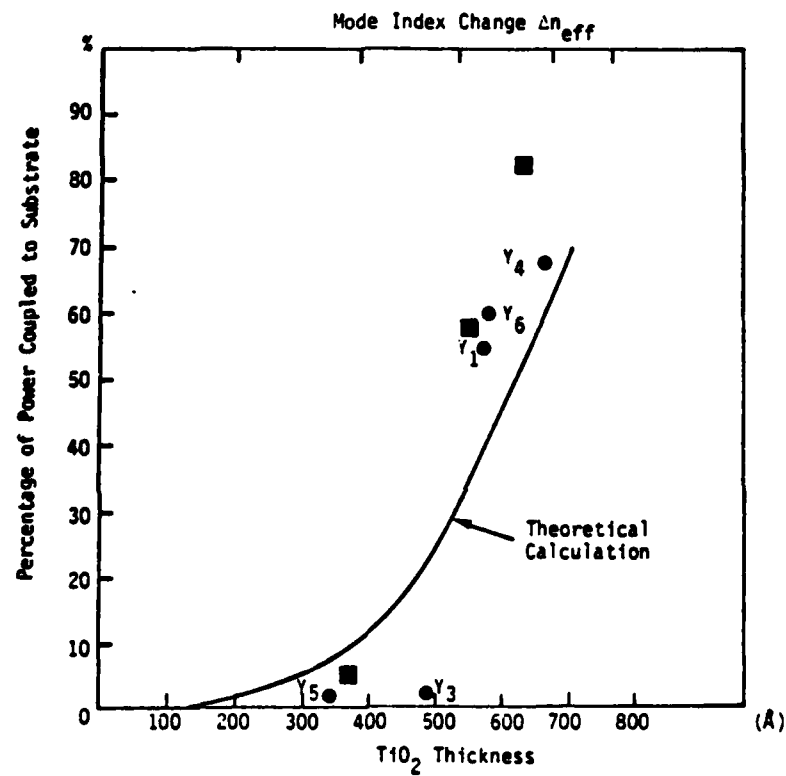


● Experimental results when water is at 95°C during diffusion.

▲ Experimental results when water is at room temperature (25°C).

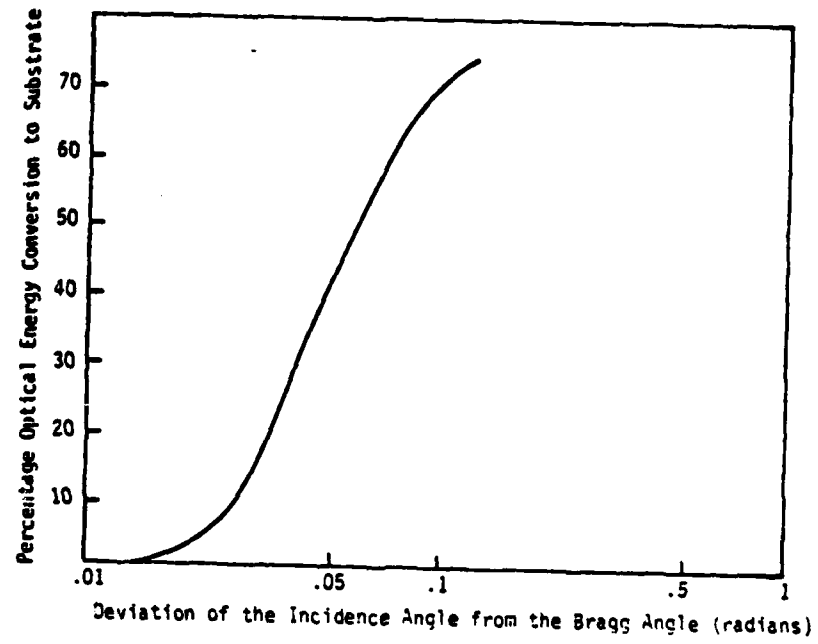


- Experimental results when water is at 95°C during diffusion.



- Experimental data for constant period gratings  
 $d = 100 \mu\text{m}$ ,  $\Lambda = 3 \mu\text{m}$ .
- Experimental data for  $100 \mu\text{m}$  wide TlO<sub>2</sub> pads.





## CHAPTER IV

Chirped Grating Lenses on  $\text{Nb}_2\text{O}_5$  Transition Waveguides

by

Siamak Forouhar, Ron-Xin Lu and William S. C. Chang  
Department of Electrical Engineering and Computer Sciences  
C-014, University of California, San Diego  
La Jolla, CA 92093

Richard L. Davis\*  
Motorola  
8201 East McDowell Road  
Scottsdale, AZ 8525  
and

Shih-Kay Yao  
TRW Technology Research Center  
2525 E. El Segundo Blvd.  
El Segundo, CA 90245

\* Dr. R. L. Davis is presently at Northrop Research and Technology Center,  
One Research Park, Rolling Hills Estate, CA 90274.

Abstract

Efficient tapered  $\text{Nb}_2\text{O}_5$  transition waveguide obtained by reactive sputtering has been demonstrated experimentally. It provides effective interconnection between two sections of Ti-indiffused waveguide with 0.8 dB total insertion loss. Chirped grating lenses have also been fabricated on  $\text{Nb}_2\text{O}_5$  waveguides that have yielded 85% throughput efficiency. For signal processing applications in Ti-indiffused waveguides, the combination of grating lenses and the  $\text{Nb}_2\text{O}_5$  transition waveguide will allow us to obtain lens functions that have both high efficiency and large angular field of view ( $\sim 4^\circ$ ).

## 1. INTRODUCTION

Chirped grating lenses on glass optical waveguides (Figure 1) have been fabricated successfully with high throughput efficiency, several degrees angular field of view, and near diffraction-limited performance [1,2]. However for some signal processing applications, such as the r.f. spectrum analyzer, it is necessary to fabricate grating lenses on  $\text{LiNbO}_3$  waveguides. Recently, the theoretical design and fabrication of diffraction grating lenses on single mode Ti-indiffused  $\text{LiNbO}_3$  waveguides were reported [3,4].

The experimentally-measured performance of chirped grating lenses on Ti-indiffused waveguides indicates that it is difficult to get both high efficiency and more than two degrees of angular field of view for two reasons. (a) The mode index of Ti-indiffused  $\text{LiNbO}_3$ ,  $n_e$ , is close to the substrate index,  $n_s$ . Therefore, the coupling of the energy to the substrate may limit the maximum angular field of view or the efficiency of small  $F$  number grating lenses [5]. (b) The Ti-indiffused  $\text{LiNbO}_3$  waveguides have large mode depth (typically 1.5 - 2.5  $\mu\text{m}$ ). The large mode depth implies a small coupling coefficient, thus requiring long grating grooves which limit the angular field of view. In order to improve the grating lens performance, an alternative waveguide in  $\text{LiNbO}_3$  other than Ti-indiffused is needed that has smaller mode depth and larger mode index. If Ti-indiffused  $\text{LiNbO}_3$  must be used for other signal processing functions, such as acousto-optic interaction in the r.f. spectrum analyzer, then the alternate waveguide may be used as a transition waveguide interconnecting two sections of Ti-indiffused regions for the grating lens fabrication as shown in Figure 2.

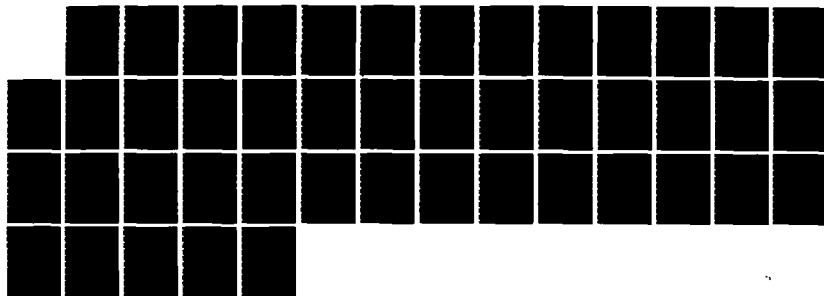
AD-A137 103

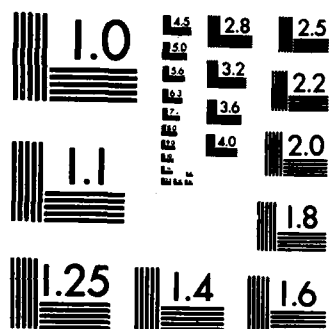
FABRICATION AND EVALUATION OF CHIRPED GRATING LENSES IN 2/2  
LITHIUM NIOBATE W. (U) CALIFORNIA UNIV SAN DIEGO LA  
JOLLA DEPT OF ELECTRICAL ENGINEE. S FOROUHAR ET AL.

UNCLASSIFIED

01 OCT 83 AFOSR-TR-83-1314 AFOSR-80-0037 F/G 20/6

NL





MICROCOPY RESOLUTION TEST CHART  
NATIONAL BUREAU OF STANDARDS-1963-A

## 2. $\text{Nb}_2\text{O}_5$ Interconnection Waveguides

The formation of light-guiding interconnections on glass waveguides was first demonstrated by P. K. Tien [6]. However it was thought that such structures would result in a relatively high loss if used on  $\text{LiNbO}_3$  substrates due to the surface roughness of commercially-available  $\text{LiNbO}_3$  crystals [7]. Since then, fabrication of very low loss (less than 0.5 dB/cm)  $\text{Nb}_2\text{O}_5$  films on  $\text{LiNbO}_3$  substrates has been reported [8]. As an alternative approach to improve the performance of chirped grating lenses on Ti-indiffused  $\text{LiNbO}_3$ , we have investigated the feasibility of such interconnections on  $\text{LiNbO}_3$  substrates using  $\text{Nb}_2\text{O}_5$  films. Figure 2 shows the cross-section of a y-cut  $\text{LiNbO}_3$  crystal with two Ti-indiffused guiding regions that have been connected by a  $\text{Nb}_2\text{O}_5$  film. Since the refractive index of the  $\text{Nb}_2\text{O}_5$  film ( $n = 2.24$  to  $2.28$ ) is larger than the refractive index of the Ti-indiffused layers, a much larger angular field of view and smaller F number may be expected for grating lens structures fabricated on the  $\text{Nb}_2\text{O}_5$  waveguides.

## 3. $\text{Nb}_2\text{O}_5$ Film Fabrication

The niobium pentoxide films were formed by reactively sputtering a high purity niobium metal target in an oxygen-argon atmosphere. This is a widely used technique for forming a variety of metal oxide waveguides, and has resulted in  $\text{Nb}_2\text{O}_5$  waveguides exhibiting high refractive index ( $n = 2.26$

at Motorola and  $n = 2.24$  at UCSD at  $\lambda = .633 \mu\text{m}$ ) and low optical loss. It should be noted that the optical properties of  $\text{Nb}_2\text{O}_5$  waveguides have been found to be very sensitive to the conditions under which they are deposited [9] necessitating stringent control of the deposition environment to insure reproducible results. The  $\text{Nb}_2\text{O}_5$  films at Motorola are deposited in an r.f. diode system using a 15 cm diameter x .5 cm thick MARZ grade niobium metal target. Both target and substrate platforms are water-cooled and are separated by approximately 8 cm. After the sputtering chamber has been evacuated, the high vacuum pump is throttled down and oxygen and argon are introduced through separate micrometer needle valves. The partial pressures of the gases are 1 millitorr  $\text{O}_2$  and 3 millitorr Ar. Low chamber pressure during the process tends to result in better quality waveguides but further reduction in the total pressure results in the inability to maintain a stable discharge at the r.f. power levels used. The depositions were made with 75 watts ( $.41 \text{ W/cm}^2$ ) of r.f. power. The cathode (target) assumed a bias potential of 720 volts and the substrate was allowed to float with respect to ground. As noted by Ingrey and Westwood [10], the low power level is dictated by the relatively low melting temperature of the pentavalent oxide phase and film growth. The combination of low pressure and low power results in a deposition rate of about  $750 \text{ \AA/hr}$ . Films grown under these conditions exhibit no evidence of crystallinity under x-ray diffraction analysis. Prior to deposition, the  $\text{LiNbO}_3$  substrates were prepared as follows. First they were scrubbed with a detergent and rinsed. This rinse, as were all subsequent rinses, was done in high resistivity de-ionized water. Next they were placed in a room temperature stripping solution of chromic and sulfuric acids for 5 to 10 seconds and rinsed. Then they were gently agitated

in a detergent solution followed by a thorough rinsing. Finally, a succession of 30 second baths in acetone, TCA, and acetone again was followed by a final rinsing. The substrates then were spun dry and immediately placed in the sputtering chamber. 2 inch diameter oxidized silicon wafers were also placed in the chamber and the films deposited on these wafers were analyzed for refractive index and optical loss. A qualitative assessment of these films indicated propagation losses of less than 1 dB/cm which was subsequently confirmed by quantitative measurements of the films on the  $\text{LiNbO}_3$  substrates. The film refractive index was determined by prism coupling .633  $\mu\text{m}$  radiation from a HeNe laser to the various waveguide modes and measuring the mode launch angles. The mode spectra was then fit to a step index waveguide dispersion diagram. At Motorola, we measured a refractive index of  $2.278 \pm .005$  for the films grown on the oxidized silicon substrates. The films on the  $\text{LiNbO}_3$  substrates exhibited a refractive index of only  $2.258 \pm .005$ .

#### 4. $\text{Nb}_2\text{O}_5$ Taper Formation and Evaluation

An extensive amount of research has been carried out in controlling the profile of sputtered films for the fabrication of integrated optics devices such as Luneberg lenses [11]. Edges with long tapers and very gentle slopes can be obtained by undercutting the bottom surface of the shadowing masks. Milton et al. [12] have developed theories to calculate the optimum taper length for an adiabatic transition of power in branching waveguides that may be used to

optimize the taper performance. We have experimentally studied and evaluated several taper profiles using glass shadow masks during the sputtering process. Glass masks, instead of metal masks, are used in order to avoid perturbation of the electric field. Figure 3 shows the mask configuration used during the deposition process and the thickness variation of two transition waveguides measured by a Dektak. The insertion loss of tapered interconnections are measured by placing the input prism coupler on side A of the Ti-indiffused waveguide and the output prism on side B as illustrated in Figure 2. The total insertion loss is the logarithm of the ratio of the power detected on side B to the power that would have been detected by the output coupler if the Ti-indiffused waveguide were continuous with no  $\text{Nb}_2\text{O}_5$  interconnection. All the Ti-indiffused waveguides were evaluated before the deposition of interconnection regions. Without the interconnection waveguides, all of the guided-wave energy coupled into side A was lost to the substrate and no guided energy was detected at the B side of the Ti-indiffused guides. Some of the measured results with the tapered interconnection  $\text{Nb}_2\text{O}_5$  waveguide are listed in Table 1. The lowest insertion loss measured was 0.8 dB when the two sections of the Ti-indiffused waveguides were separated by 1 mm. The shadow mask used during the sputtering of  $\text{Nb}_2\text{O}_5$  was 1 mm thick with the undercutting angle of  $30^\circ$ . However, the refractive index of the  $\text{Nb}_2\text{O}_5$  film in the interconnection region is between the ordinary and the extraordinary indices of  $\text{LiNbO}_3$  substrate. The propagation characteristics of any TE mode propagating in a direction  $\alpha$  from the x-axis may be approximated by an isotropic step index waveguide that has a film index of 2.26 and substrate index of  $(n_e^2 \cos^2 \alpha + n_o^2 \sin^2 \alpha)^{1/2}$  where  $n_e$  and  $n_o$  are the extraordinary and ordinary indices of  $\text{LiNbO}_3$  crystal respectively. The TE mode of such an isotropic step index waveguide will be beyond cut-off at some  $\alpha$  value equal to  $\alpha_c$ . Therefore we would expect that the insertion loss of the interconnection to increase as the

guided wave propagation direction deviates from the ordinary axis of the  $\text{LiNbO}_3$  crystal, i.e. the x-axis. The increase of the insertion loss may also be partly due to leaky mode for Ti-indiffused waveguide [13]. The measured insertion loss as a function of the angular deviation of the propagation direction with respect to the x-axis is illustrated in Figure 4. Larger indices of the  $\text{Nb}_2\text{O}_5$  film in the interconnection region will reduce the dependence of the insertion loss on the angular deviation.

A parameter that may limit the usefulness of such interconnections for applications such as the r.f. spectrum analyzer is the amount of the in-plane scattering introduced by the taper edges. Figure 5 shows the angular spectrum of the guided-wave energy at  $\lambda = .6328 \mu\text{m}$  coupled out of a Ti-indiffused  $\text{LiNbO}_3$  waveguide by a prism coupler without any interconnection waveguide. The guided-wave energy is excited by an input prism coupler using a HeNe laser. Thus the measured inplane scattering includes that of the prism couplers. Figure 6 shows the angular spectrum of the guided-wave energy coupled out after passing through the  $\text{Nb}_2\text{O}_5$  interconnection region. The same prism couplers were used for both measurements. As seen from the two Figures, an addition of 10 to 15 dB of scattered noise has been introduced due to the  $\text{Nb}_2\text{O}_5$  transition. However, since no special care had been undertaken to minimize the amount of the scattering loss in our tapered connection, we believe that a much lower scattering loss can be achieved when the taper slopes and lengths are optimized.

##### 5. Grating Lens Fabrication on $\text{Nb}_2\text{O}_5$ Waveguides

Experimentally, we have investigated different processes for the fabrication of the chirped grating grooves on  $\text{Nb}_2\text{O}_5$ - $\text{LiNbO}_3$  waveguides that will yield large coupling coefficient values. The fabrication of  $\text{TiO}_2$  grating

grooves [14] on  $\text{Nb}_2\text{O}_5$  films failed because the  $\text{Nb}_2\text{O}_5$  refractive index and loss dramatically changed after the Ti-oxidation process at  $450^\circ\text{C}$ . Thus the grating grooves must be fabricated by etching. The reactive ion beam etch technique (RIE) using freon gas was employed to etch the grating grooves in the  $\text{Nb}_2\text{O}_5$  film. Variation of the  $\text{Nb}_2\text{O}_5$  etching rate as a function of the ion beam current density is illustrated in Figure 7. We have etched up to  $4000 \text{ \AA}$  of  $\text{Nb}_2\text{O}_5$  film with good pattern resolution of the grating grooves using Shipley AZ 1350 photoresist masks. Figure 8 shows the calculated coupling coefficient as a function of the groove depth on the  $\text{Nb}_2\text{O}_5$  waveguide. Clearly, fairly large  $K_c$  can be expected with a moderate depth of etching. We have fabricated several lenses on  $\text{Nb}_2\text{O}_5$ - $\text{LiNbO}_3$  waveguides. The specifications of the mask pattern used are:  $\lambda_{\min} = 1.73 \text{ }\mu\text{m}$ ,  $\lambda_{\max} = 3.45 \text{ }\mu\text{m}$ , focal length ( $f$ )  $\approx 12 \text{ mm}$ , grating groove length  $d = 40 \text{ }\mu\text{m}$ , lens width ( $h$ )  $= 1 \text{ mm}$ , and F number  $\approx 12$ . The highest throughput efficiency measured for the above lens was  $85 \pm 5\%$  for the groove depth of  $\approx 2000 \text{ \AA}$ . The efficiency measurements were made by prism couplers. The throughput efficiency is the ratio of power measured in the diffracted beam focused at the focal point to the power measured in the guided-wave beam transmitted through the waveguide when the transverse location of the incident beam is moved to bypass the lens. The diffraction efficiency is the ratio of the power measured in the focused beam to the sum of the powers measured in all the orders of diffraction. For the lenses fabricated on  $\text{Nb}_2\text{O}_5$  films, the diffraction efficiency was equal to the throughput efficiency, implying that very little power was converted by the lens to the substrate modes. The measured angular field of view for the lens was  $\Delta\theta \approx 4^\circ$ . The angular field of view,  $\Delta\theta$ , is the change in the incidence angle within which the measured efficiency is larger than one half of the highest efficiency.

## 6. Conclusions

The feasibility of using a  $\text{Nb}_2\text{O}_5$  transition waveguide to interconnect two separate sections of Ti-indiffused waveguide has been demonstrated with a total insertion loss of 0.8 dB. The key to the low loss transition is a very smooth taper obtained by sputtering using a glass shadow mask.  $\text{Nb}_2\text{O}_5$  waveguides obtained by reactive sputtering of Nb in an  $\text{O}_2$ -Ar atmosphere has a propagation loss less than 1 dB/cm in the x or the y direction. The chirped grating lens fabricated on top of such a waveguide by reactive ion beam etching has an 85% throughput efficiency and four degrees of angular field of view. Thus, the combination of the tapered transition waveguide and the grating lens will allow us to obtain the lens function with high efficiency and large angular field of view for any signal processing applications using Ti-indiffused  $\text{LiNbO}_3$  without the disadvantages of the deep mode depth and small  $n_e - n_s$  value. Such a technique may also be used to modify the mode profile of Ti-indiffused waveguides in other applications such as butt coupling, directional coupling or switching. It has two drawbacks.

- (1) The propagation loss increases as the direction of propagation is moved away from the x or the y axes because the ordinary index of  $\text{LiNbO}_3$  is larger than the index of the  $\text{Nb}_2\text{O}_5$  film.
- (2) The  $\text{Nb}_2\text{O}_5$  waveguide will be affected severely by any subsequent processing that has a temperature higher than 400°C.

7. Acknowledgement

This work is supported in part by AFOSR Grant No. 80-0037 with the University of California, San Diego.

# REFERENCES

1. J.-M. Delavaux, S. Forouhar, W. S. C. Chang, and R.-X. Lu, "Experimental Fabrication and Evaluation of Diffraction Lenses in Planar Optical Waveguides", *IEEE/OSA Conference on Lasers and Electro-optics, Phoenix, Arizona*, (April 1982).
2. S. K. Yao and D. E. Thompson, *Appl. Phys. Lett.*, **33**, 635 (1978).
3. Z.-Q. Lin, S.-T. Zhou, W. S. C. Chang, S. Forouhar, and J.-M. Delavaux, *MIT Transactions*, **MTT-29**, 881 (1981).
4. W. S. C. Chang, S. Forouhar, J.-M. Delavaux, and R.-X. Lu, "Chirped Grating Lenses in Ti-indiffused LiNbO<sub>3</sub> Optical Waveguides", *Proc. European Conference on Optical Systems and Applications, Edinburgh, Scotland*, 7 - 10 Sept. 1982, to be published.
5. S. K. Yao, *SPIE Integrated Optics Proceedings*, **269**, (February 1981).
6. P. K. Tien, R. J. Martin, and G. Smolinsky, *Appl. Opt.*, **12**, 224 (1973).
7. H. P. Hsu and A. F. Milton, *IEEE J. Quantum Electron.*, **QE-13**, 224 (1975).
8. R. L. Davis, "RF Sputtered Thin Film Niobium Pentoxide for Integrated Optics", *American Vacuum Society Symposium, Scottsdale, Arizona*, (February 1982).
9. R. L. Davis and F. S. Hickernell, "Thin Film Oxides of Vanadium, Niobium, and Tantalum for Integrated Optics", *SPIE Technical Symposium East, Washington, D.C.*, (April 1983).
10. S. J. Ingray and W. D. Westwood, *Appl. Opt.*, **15**, 607 (1976).
11. S. K. Yao, D. B. Anderson, C. M. Oaria, and V. G. Kreismanis, "Mask Synthesis for Diffraction Limited Waveguide Luneberg Lenses", *Optical Engg. on Integrated and Guided Wave Optics, Salt Lake City, Utah*, (January 1977).

12. A. F. Milton and W. K. Burns, *Appl. Opt.*, 15, 1207 (1975).
13. W. A. Burns, S. K. Sheem, and A. F. Milton, *IEEE J. Quantum Electron.*, QE-15, 1282 (1979).
14. S. Forouhar, C. Warren, R.-X. Lu, and W.S. C. Chang, "Techniques for the Fabrication of High-index Overlay Films on  $\text{LiNbO}_3$ ". *SPIE Technical Symposium, Arlington, Virginia*, (April 1983).

TABLE 1: The Total Nb<sub>2</sub>O<sub>5</sub> Waveguide Interconnection Loss and Taper Transition Slopes of Four of the Samples Made at UCSD and Motorola.

Distance Between Two Ti-Indiffused Regions (mm)	Nb <sub>2</sub> O <sub>5</sub> Interconnection Length (mm)	Maximum Taper Slope (milliradians)	Insertion Loss (dB)
1.	4.4	.54	-0.8 (UCSD)
2.	6.3	.54	-1.4 (Motorola)
2.	5.1	1.8	-2.5 (Motorola)
2.	5.6	1.8	-7.0 (UCSD)

Here, the guided-wave mode is propagating in the  $x$  direction and is incident at an angle approximately perpendicular to the tapered edge of the Nb<sub>2</sub>O<sub>5</sub> transition waveguide.

### List of Figures

Figure 1: Bragg Diffraction Chirped Grating Lens.

Figure 2: The  $\text{Nb}_2\text{O}_5$  Transition Waveguide.

Figure 3: (a) The Configuration of the Shadow Mask during Sputter Deposition of  $\text{Nb}_2\text{O}_5$  Film.

(b) The Thickness Profile of a  $\text{Nb}_2\text{O}_5$  Transition Waveguide Measured by the Dektak.

Figure 4: The Measured Insertion Loss of a  $\text{Nb}_2\text{O}_5$  Waveguide as a Function of the Angular Deviation of the Propagation Direction with Respect to the Ordinary Axis.

Figure 5: In-Plane Scattering Intensity of the Guided Wave Energy Coupled Out of a Ti-indiffused  $\text{LiNbO}_3$  Waveguide without any Interconnection Intensity.

Figure 6: In-Plane Scattering Intensity of the Guided Wave Energy Coupled Out After Passing Through the  $\text{Nb}_2\text{O}_5$  Interconnection Region.

Figure 7: Variation of Etching Rate of  $\text{Nb}_2\text{O}_5$  Film as a Function of Ion Beam Current Density.

Figure 8: Coupling Coefficient vs. Etching Depth of a  $\text{Nb}_2\text{O}_5$  Film with Refractive Index of 2.26 on  $\text{LiNbO}_3$  Substrate.

The  $\text{Nb}_2\text{O}_5$  Film Thickness of the Waveguide is 7000 Å.

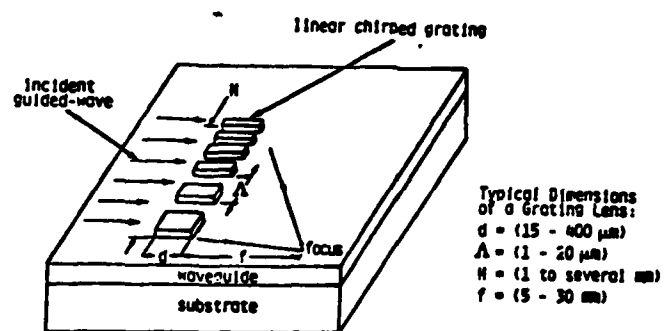
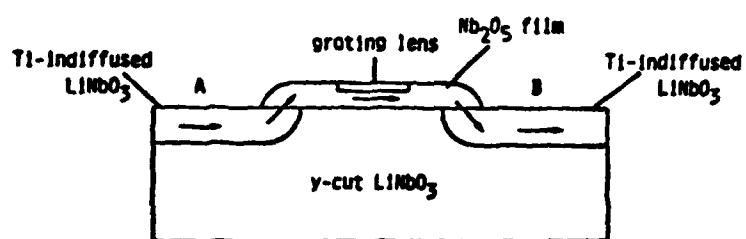
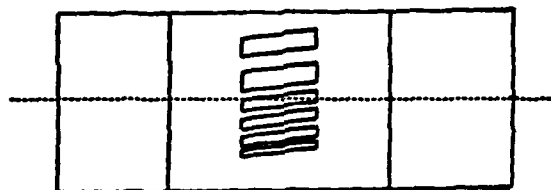


Figure 1

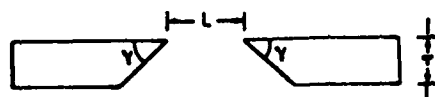


Side View of Mode-Lift-Off Structure

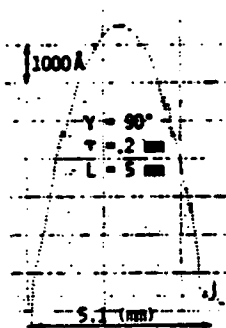
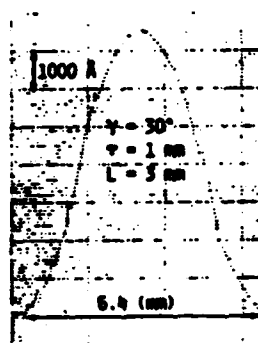


Top View of Mode-Lift-Off Structure

Figure 2



(a)



(b)

Figure 3

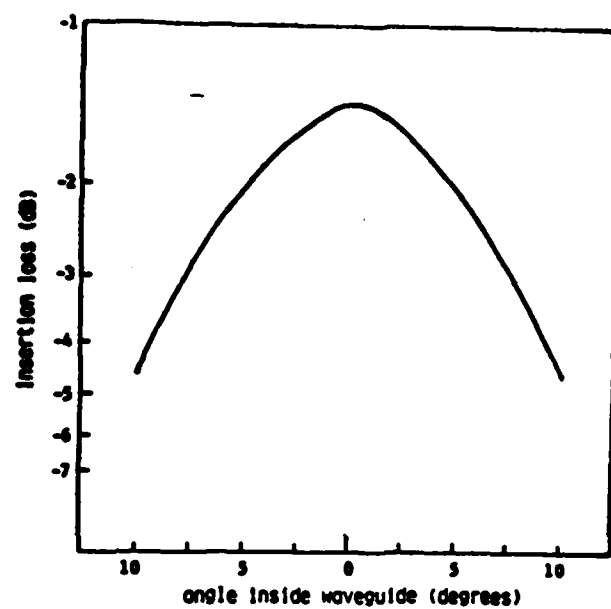


Figure 4

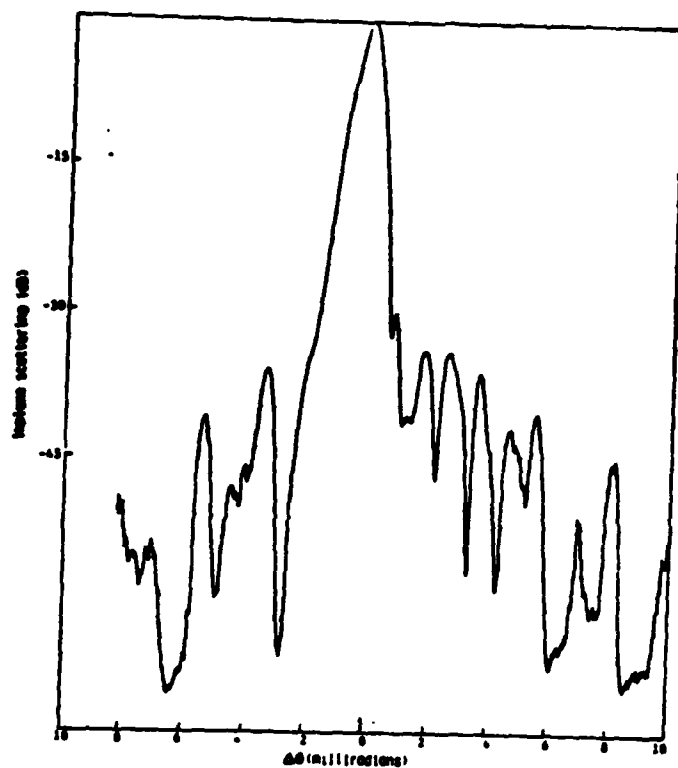


Figure 5

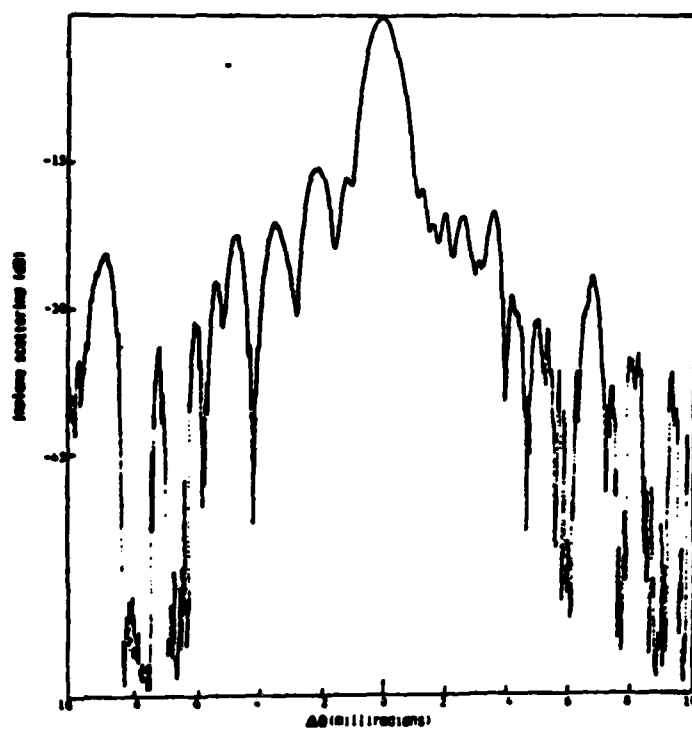


Figure 6

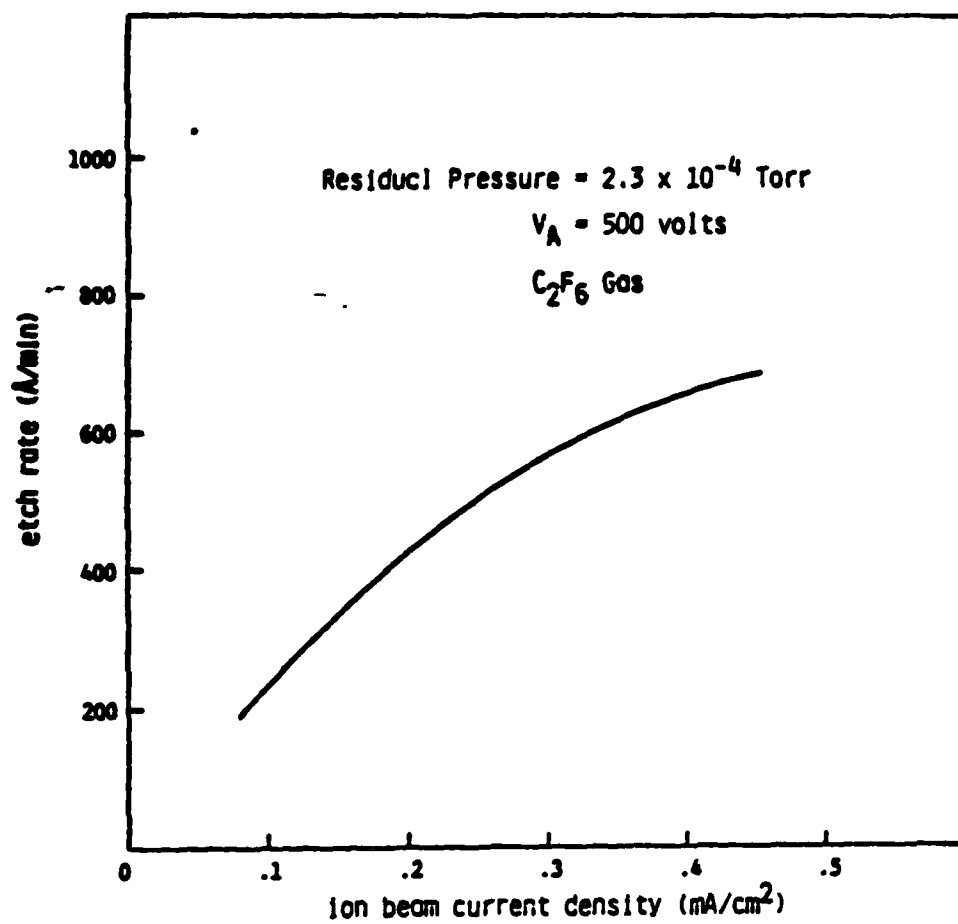


Figure 7

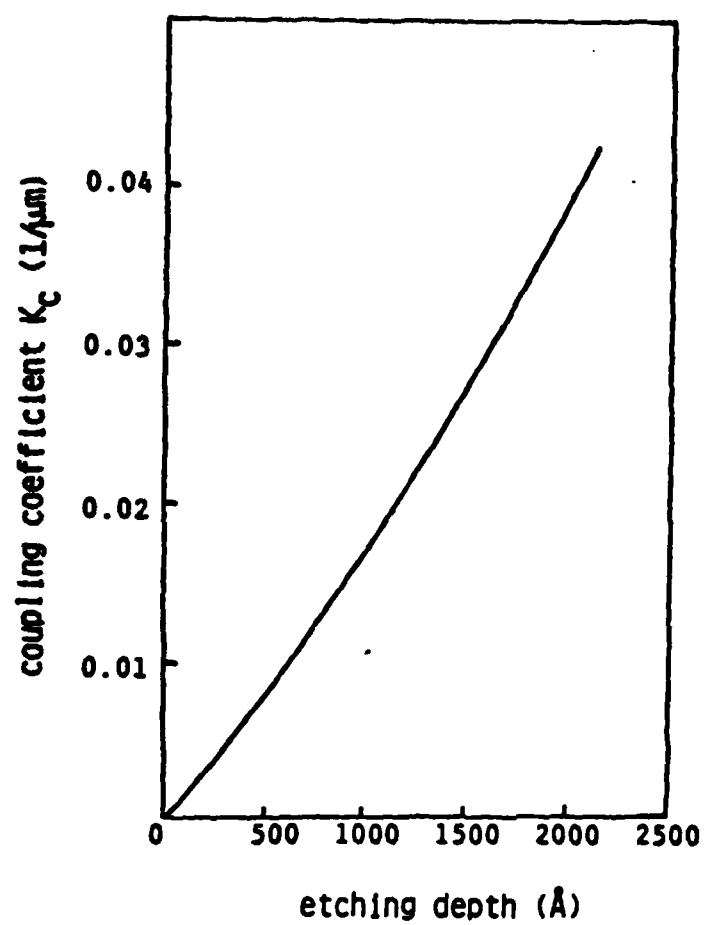


Figure 8

**CHAPTER V**

Double Ion Exchanged  
Chirp Grating Lens in Lithium Niobate Waveguides

by

Christopher Warren, Siamak Forouhar and William S. C. Chang  
C-014, Department of Electrical Engineering and Computer Sciences  
University of California, San Diego  
La Jolla, CA 92093  
Tel: 619-452-2737

and

S. K. Yao  
TRW Technology Research Center  
2525 E. El Segundo Blvd.  
El Segundo, CA 90245

Abstract

An integrated optical chirped grating lens has been produced which exhibits high throughput efficiency (75%) and large angular field of view (3 degrees). The waveguide substrate is x-cut lithium niobate, and ion exchange in benzoic acid is the method used for making the lens and the waveguide.

Chirped grating lenses on glass optical waveguides have been fabricated successfully with 90% diffraction efficiency, several degrees angular field of view, and near diffraction limited performance [1,2]. However, for some signal processing applications, such as the r.f. spectrum analyzer, it is necessary to fabricate these lenses on  $\text{LiNbO}_3$  waveguides. The fabrication and performance of chirped grating lenses on commonly used  $\text{LiNbO}_3$  waveguides, i.e. Ti-indiffused  $\text{LiNbO}_3$ , has recently been reported [3], and a throughput efficiency of 60% with  $2^\circ$  angular field of view was obtained. However, the combination of high efficiency and large angular field of view for chirped grating lenses on Ti-indiffused  $\text{LiNbO}_3$  waveguides is difficult to obtain due to two reasons:

- a. The mode index of Ti-indiffused  $\text{LiNbO}_3$ ,  $n_e$ , is close to the substrate index,  $n_s$ , so the substrate mode coupling may limit the maximum angular field of view or the efficiency of small F-number grating lenses.
- b. The Ti-indiffused  $\text{LiNbO}_3$  waveguides have large mode depth [3]. The large mode depth implies small coupling coefficient, thus a large diffraction efficiency grating requires long grating grooves which limit the angular field of view.

Furthermore, since lithium niobate has a high index, the overlay film material used for grating must have an even higher index in order to obtain large coupling coefficient at small film thicknesses.

In order to improve the chirped grating lens performance and relax the limitation imposed by the Ti-indiffused  $\text{LiNbO}_3$  waveguides, we have investigated the single mode waveguide in  $\text{LiNbO}_3$  made by proton ion exchange [4]. Compared to the Ti-indiffused waveguide, it has smaller mode depth and larger mode index. We have obtained higher performance chirped grating lenses on an ion-exchanged waveguide by a second ion exchange process.

A typical chirped grating lens is illustrated in Figure 1. There are several factors which one should consider when choosing a particular chirped grating lens design. From the generalized coupled mode theory [5], in order to have a large diffraction efficiency we can choose  $Kd = \pi/2$  where  $K$  is the coupling coefficient and  $d$  is the grating groove length. The coupling coefficient is directly related to the change in effective index,  $\Delta n_g$ , in the waveguide caused by the grating grooves. In the case of small effective index perturbations this relationship is given by [5]  $K = \pi \Delta n_g / \lambda$ .

Another requirement that must be satisfied for large diffraction efficiency is that the gratings must not scatter heavily into either the higher diffraction orders or the substrate modes. A common figure of merit in this regard for constant periodicity grating is the dimensionless parameter  $Q$  [6],  $Q = 2\pi\lambda d / (n_g \Lambda^2)$ , where  $\lambda$  = free space wavelength and  $\Lambda$  = periodicity of grating. For a chirped grating where  $\Lambda$  is variable, we shall have a local  $Q$ -factor for various sections of the lens. For most of our designs, we have kept the local  $Q$  value larger than 5 so that the energy diffracted into higher orders may be ignored. Optical loss due to conversion into the substrate modes can be minimized if  $n_g$  can be made significantly larger than  $n_s$ .

A third consideration in lens design is the angular field of view,  $\Delta\theta$ . From the conventional coupled mode theory, the  $\Delta\theta$  of a constant periodicity grating is given by  $\Delta\theta \approx \Lambda/d$  [6]. This relationship can still serve as a useful qualitative guide for the design of a chirped grating lens. For large  $\Delta\theta$ , we want  $\Lambda/d$  large. But for large  $Q$ , we want  $d/\Lambda^2$  large. Thus, we should use as small a  $\Lambda$  as the resolution of the lithographic process allows, while using a large enough  $K$  such that the optimum  $d$  for high efficiency is still small enough to support large  $\Delta\theta$ , yet is not so small for  $Q$  to become too low.

As was mentioned previously, substrate mode coupling in Ti-indiffused waveguides may limit the efficiency of small F-number grating lenses. This is because for small F-number a significant portion of the input beam will not be at Bragg angle due to the chirped periodicity of the grating. In other words, only within a small range of  $\lambda$  along the lens (usually at the middle) will Bragg's diffraction condition be satisfied approximately. For significant deviations from Bragg angle, there will be substrate mode conversion if the mode index,  $n_g$ , of the waveguide is not significantly larger than the substrate index,  $n_s$ .

The proton ion exchange process is expected to give an  $n_g$  significantly higher than  $n_s$ . The second proton ion exchange is expected to give a large K for the grating grooves. Thus, high performance chirp grating lens can be expected with a double proton ion-exchange process.

The ion exchange method used here involves dipping a sample of x-cut  $\text{LiNbO}_3$  in molten benzoic acid [4] held in a furnace that has a  $\pm 1^\circ$  temperature control. Some of the protons from the acid diffuse into the lithium niobate and replace some of the lithium ions in the crystal. The result is that a thin surface layer of the crystal acquires a constant refractive index of 2.32, which is large compared to the substrate index, 2.20 (at  $\lambda = .6328 \mu\text{m}$ ). This index profile and index value can be determined by fitting the index profile with measured effective indices of a multimode waveguide by WKB approximation. The temperature and duration of immersion control the depth of this layer, the mode indices, and the number of modes. We work strictly in the single mode region. In Figure 2, a theoretical curve of  $\text{TE}_0$  mode index versus time of immersion at  $217^\circ\text{C}$ , is given, based upon Jackel's reported diffusion coefficient of  $.37 \mu\text{m}^2/\text{hr.}$ , as well as two other values of diffusion coefficients for comparison. The discrete points are

the experimentally observed waveguide index,  $n_g$ . They are approximately in agreement.

An aluminum mask in the form of chirped grating grooves is made on the single-mode ion exchanged waveguide by the lift-off method, contact printed from a flexible chromium mask. The aluminum serves as a protective mask during the second ion exchange. For the second ion exchange, the waveguide is immersed in benzoic acid for a few minutes at 204°C. Thus, the majority of the planar waveguide is double ion exchanged, while the regions beneath the aluminum fingers is single ion exchanged. After the second ion exchange the aluminum mask is removed by chemical etching.

Double ion exchange produces a change in  $n_g$  from the single ion exchange. In order to measure  $\Delta n_g$ , we have set aside a portion of the waveguide which is also covered by aluminum during the second ion exchange.

$\Delta n_g$  is measured by the change in coupling angles of the light beam into the rutile prism in the single exchanged region and in the double exchanged region. A theoretical curve of  $\Delta n_g$  versus second ion exchange time is plotted in Figure 3 using  $D = .12 \mu^2/\text{hr}$ . The experimental points are marked by the squared dots. Clearly there are some variations of  $\Delta n_g$  caused by some unknown variations of our experimental conditions. Nevertheless, the averaged  $\Delta n_g$  may be described by  $\Delta n_g = 0.0012 t$  where  $t$  is the second ion exchange time in minutes at 204°C.

All optical measurements are performed with a He-Ne laser through rutile prism couplers. The throughput efficiency is defined as the ratio of the optical power in the focused diffracted guided wave beam to the power in the transmitted guided optical beam when the incident beam is moved transversely to by-pass the lens. The diffraction efficiency is the ratio of the power measured in the focused beam to the sum of the powers measured in all the

orders of diffraction. So far, within the accuracy of our measurement the diffraction efficiency is always equal to the throughput efficiency, implying very little power converted by the lens into the substrate modes. However, the average attenuation rate of the single mode ion exchanged waveguide is 3 dB/cm. There are significant amounts of light power appearing in the substrate and in the tails of the output m-line, indicating that the random scattering noise of the ion exchanged waveguide will be higher than that of the Ti-indiffused waveguide.

Figure 4 shows the measured throughput efficiency  $\eta$  for various  $\Delta n_e$  created on 7 different samples. In all these samples, the  $n_e$  of the  $TE_0$  mode produced in the first ion exchange is  $2.265 \pm .005$ . The lens has the same mask pattern,  $\lambda_{\min} = 1.73 \mu\text{m}$ ,  $\lambda_{\max} = 3.45 \mu\text{m}$ , focal length ( $f$ ) = 12 mm, grating groove length  $d = 80 \mu\text{m}$ , lens width ( $h$ ) = 1 mm and  $F = 12$ . The solid curve represents the efficiency variation calculated from the generalized coupled mode theory for  $K = \pi \Delta n_e / \lambda$ . Clearly, the measured efficiency at  $\Delta n_e$  larger than 0.007 is larger than the calculated efficiency, implying an experimental  $K$  value smaller than that given by  $K = \pi \Delta n_e / \lambda$ . A reduction in  $K$  value could occur due to mechanisms such as lateral diffusion in the  $z$ -axis direction. The exact mechanism for the shift of the experimental points are still being investigated. However, the experimental results have demonstrated that the second ion exchange process is more than sufficient to generate the large  $\Delta n_e$  required for obtaining high efficiency at short  $d$  values.

By measuring the diffraction efficiency as a function of the angle of incidence of the input guided wave beam, we obtain experimentally the angular field of view  $\Delta\theta$  to be in the range from 2.4 degrees to 3.2 degrees.  $\Delta\theta$  is defined as the change in incidence angle within which the measured efficiency is larger than one half the highest efficiency. We do not know yet the exact

reason for the variation in  $\Delta\theta$ . It may be caused by the tolerance of the fabrication processes.

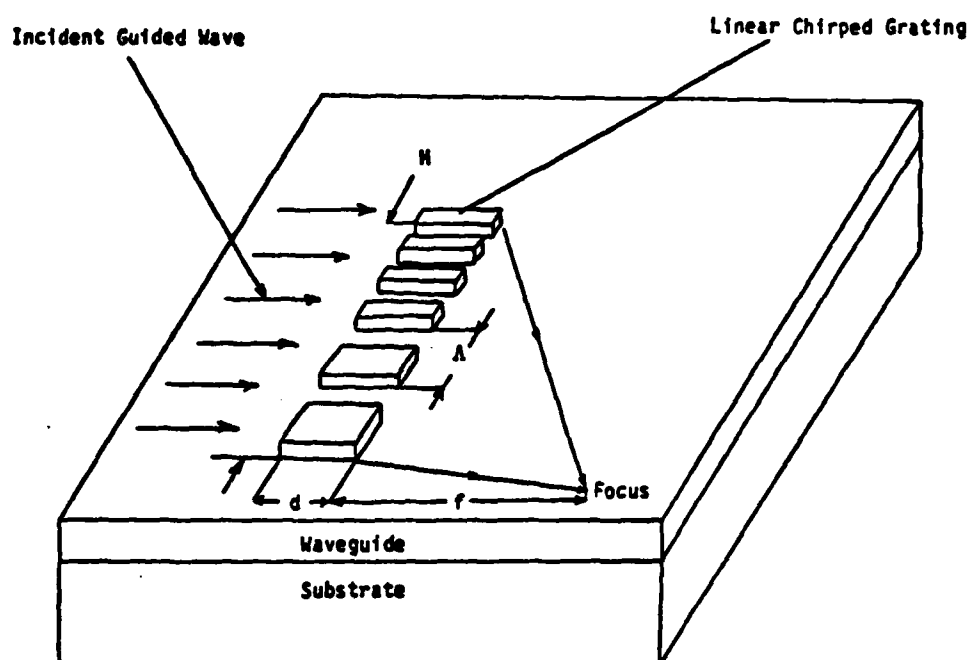
In conclusion, we have demonstrated a chirped grating lens on  $\text{LiNbO}_3$  that has high efficiency (75%) and large angular field of view (3 degrees). It is potentially feasible to obtain a higher efficiency and a larger angular field of view than the data reported here by searching for a smaller  $d$  without higher orders of diffraction and by controlling the second ion exchange more precisely to obtain the desired  $K$ . There seem to be two drawbacks to ion exchanged waveguides: (1) They have a larger scattering loss than that of the Ti-indiffused waveguides, and (2) the  $n_e$  and  $\Delta n_e$  will change if the sample is heated to 200°C. This work is supported in part by AFOSR Grant No.80-0037. The grating lens mask is made by electron beam lithography at the submicron facility of Cornell University under NSF Grant No. ECS-8200312.

References:

1. J. M. Delavaux, Siamak Forouhar, W. S. C. Chang and R. X. Lu, "Experimental Fabrication and Evaluation of Diffraction Lenses in Planar Optical Waveguides", IEEE/OSA Conference on Lasers and Electro-Optics, April 1982, Phoenix, Arizona.
2. S. K. Yao, D. E. Thompson, "Chirp-Grating Lens for Guided Wave Optics", Appl. Phys. Lett., 33(7), pp. 635-637, Oct. 1st, 1978.
3. W. S. C. Chang, Siamak Forouhar, Jean-Marc Delavaux, Christopher Warren and Ron-Xin Lu, "Chirped Grating Lenses in Ti-indiffused LiNbO<sub>3</sub> Optical Waveguides", paper presented at ECOSA '82 Conference, Edinburgh, Scotland, September 1982.
4. J. L. Jackel, C. E. Rice and J. J. Vaseika, Jr., "Proton Exchange for High Index Waveguides in LiNbO<sub>3</sub>", IEEE/OSA Topical Meeting in Integrated and Guided Wave Optics, January 1982, Pacific Grove, CA.
5. Richard P. Kenan, "Theory of Diffraction of Guided Optical Waves by Thick Holograms", J. Appl. Phys., Vol. 46, No. 10, 4545-51 (October 1975).
6. Herwig Kogelnik, Bell Syst. Tech. J. 48, 2909 (1969).

Figure Captions

- Figure 1 The chirped grating lens structure and the typical ranges of the design parameters used.
- Figure 2 The effective index of ion exchanged  $\text{LiNbO}_3$  waveguides versus time of immersion in benzoic acid,  $T = 217^\circ\text{C}$ . The dashed lines show the use of different diffusion coefficients used in theoretically modelling the waveguides.
- Figure 3 The waveguides of Figure 2 with  $n_e = 2.265 \pm .05$  were ion exchanged a second time. The change in effective index is plotted versus time of second ion exchange at  $T = 204^\circ\text{C}$ .
- Figure 4 Throughput efficiency versus  $\Delta n_e$  for the chirped grating lens made in  $\text{LiNbO}_3$  waveguides.



TYPICAL DIMENSIONS OF A GRATING LENS

- $d = (15 - 400 \text{ } \mu\text{m})$
- $A = (1 - 20 \text{ } \mu\text{m})$
- $H = (1 \text{ to several mm})$
- $f = (5 - 30 \text{ mm})$

Figure 1

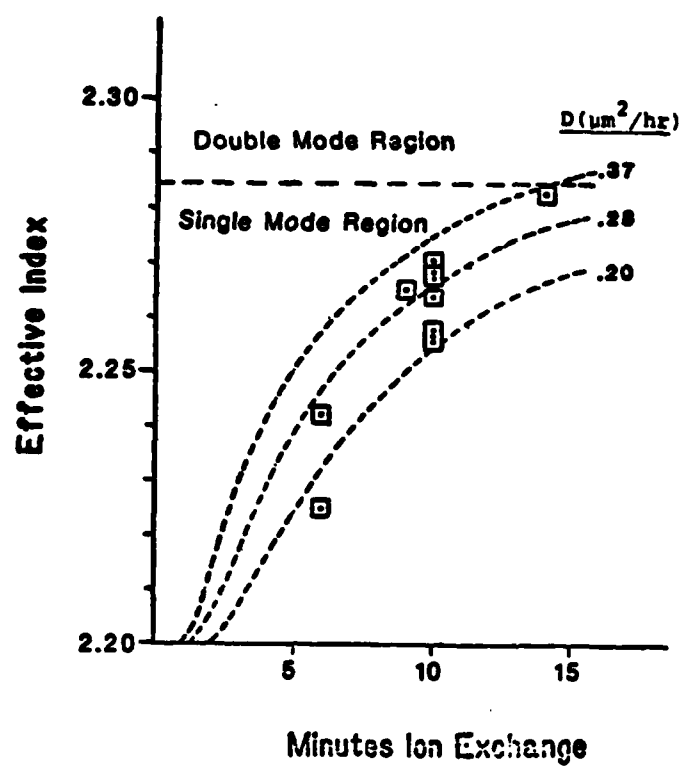


Figure 2

References:

1. J. M. Delavaux, Siamak Forouhar, W. S. C. Chang and R. X. Lu,  
"Experimental Fabrication and Evaluation of Diffraction Lenses in Planar Optical Waveguides", IEEE/OSA Conference on Lasers and Electro-Optics, April 1982, Phoenix, Arizona.
2. S. K. Yao, D. E. Thompson, "Chirp-Grating Lens for Guided Wave Optics", Appl. Phys. Lett., 33(7), pp. 635-637, Oct. 1st, 1978.
3. W. S. C. Chang, Siamak Forouhar, Jean-Marc Delavaux, Christopher Warren and Ron-Xin Lu, "Chirped Grating Lenses in Ti-indiffused LiNbO<sub>3</sub> Optical Waveguides", paper presented at ECOSA '82 Conference, Edinburgh, Scotland, September 1982.
4. J. L. Jackel, C. E. Rice and J. J. Vaseika, Jr., "Proton Exchange for High Index Waveguides in LiNbO<sub>3</sub>", IEEE/OSA Topical Meeting in Integrated and Guided Wave Optics, January 1982, Pacific Grove, CA.
5. Richard P. Kenan, "Theory of Diffraction of Guided Optical Waves by Thick Holograms", J. Appl. Phys., Vol. 46, No. 10, 4545-51 (October 1975).
6. Herwig Kogelnik, Bell Syst. Tech. J. 48, 2909 (1969).

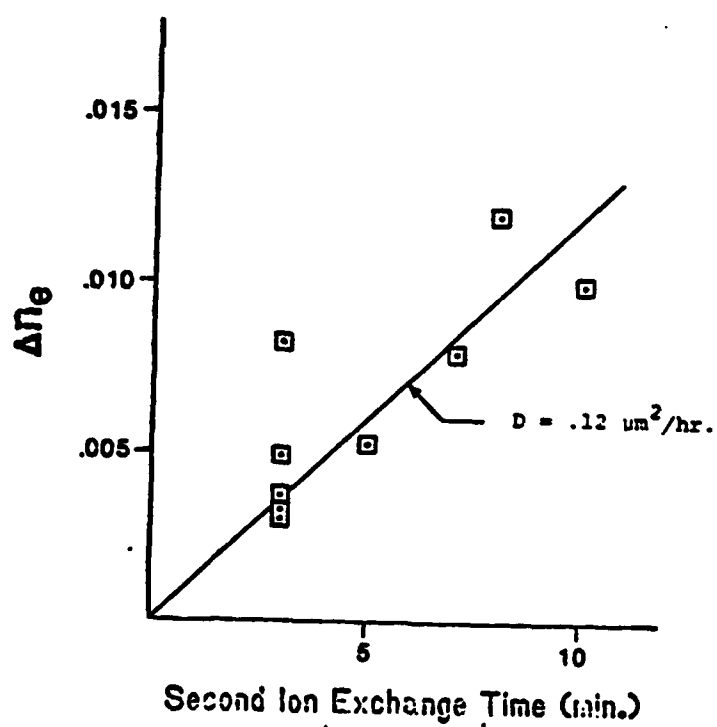


Figure 5

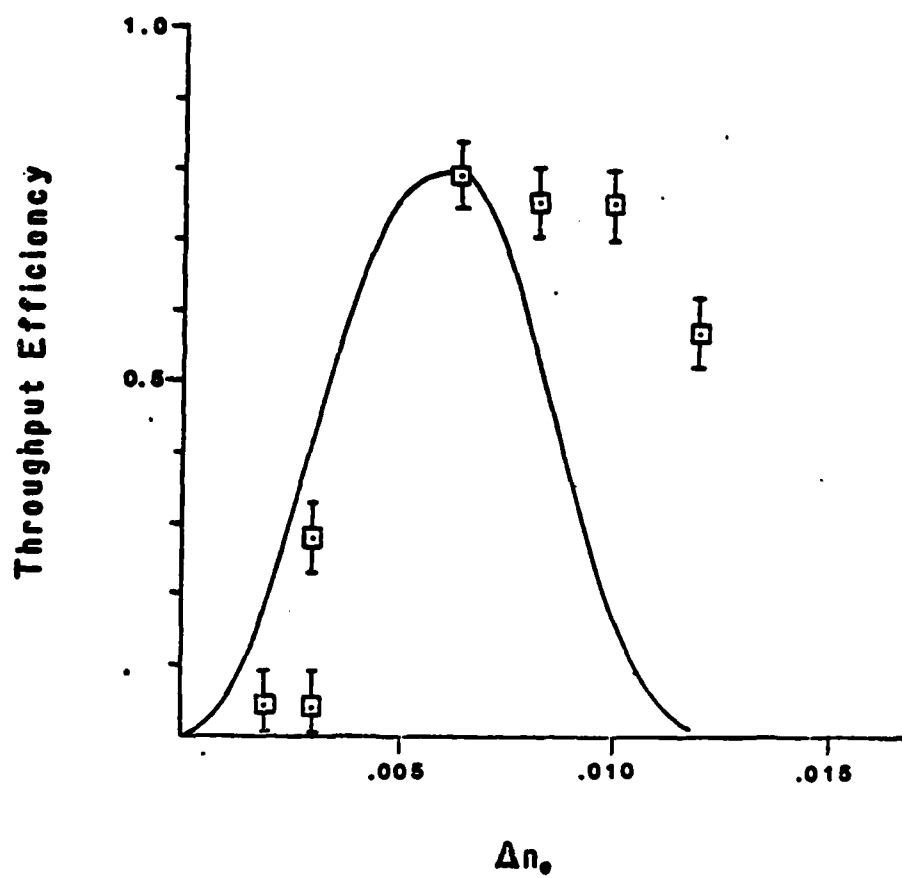


Figure 4

## CHAPTER VI

## 6. CONCLUSION

Although the investigations presented in this thesis are all concerned with the design, fabrication, evaluation and optimization of chirped grating lenses on  $\text{LiNbO}_3$  waveguides, the variations in material characteristics and fabrication techniques suggest that each segment should be considered separately. Therefore, this chapter is subdivided into four parts, each of which describes the results obtained and conclusions drawn from each chapter along with suggestions for further investigation.

6.1 The design and theoretical analysis of curved and chirped grating lenses have been performed successfully utilizing three techniques:

1. A generalized coupled mode analysis which is applicable to situations where the volume interaction is restricted only to two dominant guided wave beams. From this analysis, a general phase matching condition has been obtained that can be used to design the grating groove shape for an efficient interaction of any two guided wave beams. Alternatively, coupled mode equations have been used to calculate the phase and amplitude distributions of the two beams where there is a phase mismatch. From the calculated phase and amplitude, the diffracted field pattern, the diffraction efficiency, the angular field of view, and the effect of grating parameters for different grating lens structures have been calculated. This analysis has been found to yield good results for

structures that have high  $Q$  factors. However, the generalized coupled mode analysis does not predict the diffraction efficiency of low and medium  $Q$  structure because it neglects the presence of higher diffraction orders.

2. A perturbation method which is based upon the Green's function and is used to analyze thin phase grating structures for low  $Q$  factors. In this analysis, the effect of all diffraction orders are considered by the method of the Green's function but the effects of feedback from reversed scattering are neglected.
3. An iterative perturbation analysis which is suitable to analyze the diffraction properties of medium  $Q$  linearly chirped grating lenses. In this analysis, it is assumed that two principal guided wave beams are coupled to each other via the grating structure and the diffraction into the higher order beams is treated as losses of the two principal beams.

All the theoretical methods that have been developed assume that there is very little conversion of guided energy into the radiation modes of the optical waveguide. However, the experimental evaluations of the chirped grating lenses have demonstrated that a substantial amount of guided wave energy can couple to substrate modes when the refractive index  $n_{eff}$  of the guided wave mode is close to the substrate index. Further research is required to extend the theories so that, in addition to the guided wave modes, the radiation modes of the optical waveguides may also be incorporated in the analyzes. One way this objective may be achieved is to utilize an appropriate Green's function in the perturbation

and iterative perturbation analysis that satisfies the boundary conditions for the guided wave modes and the radiation modes of the optical waveguide.

6.2 Ti-indiffused  $\text{LiNbO}_3$  is the most important optical waveguide for integrated optics signal processing applications because of its excellent electrooptic and acoustooptic properties in conjunction with its very low propagation loss.

Etched and deposited grooved chirped grating lenses have been successfully fabricated and evaluated for the first time on Ti-indiffused  $\text{LiNbO}_3$  waveguides. A throughput efficiency of 85% for  $\text{TiO}_2$  deposited grooves and 80% for reactive ion beam etched grooves has been measured for some lenses. It has been determined that, due to the properties of Ti-indiffused  $\text{LiNbO}_3$  waveguides, it is difficult to combine high efficiency with a large angular field of view on such waveguides. There are two reasons for making this conclusion: (a) The mode index  $n_{\text{eff}}$  of Ti-indiffused  $\text{LiNbO}_3$  waveguides is very close to its substrate index  $n_{\text{sub}}$ . Therefore, any abrupt change in the structure of the optical waveguide due to the presence of the grating grooves will result in the conversion of the guided wave energy into the substrate which reduces the throughput efficiency of the grating lens. This source of loss has been investigated both experimentally and theoretically. (b) The small difference between the mode index and the substrate index causes energy leakage to the substrate modes by the grating structures at the large angle of incidence which is a limitation on the angular field of view of the grating lens.

To assess, however, the exact limitations of chirped grating

lenses on Ti-indiffused  $\text{LiNbO}_3$  waveguides, further research is required that includes:

1. The fabrication of the grating grooves by the ion exchanged process instead of etching or deposition. Due to the diffusion nature of the ion exchange, the index change caused by the grooves may be more gradual as compared to etched or deposited fingers which may result in obtaining the combination of larger efficiency and angular field of view without substantial substrate mode conversion.
2. The fabrication of  $\text{TiO}_2$  deposited fingers with tapered edges which may reduce the substrate energy conversion due to the abrupt  $\text{TiO}_2$  fingers and result in achieving larger efficiency and angular field of view for the deposited grooves.
3. The development of theoretical methods to calculate the amount of substrate mode conversion due to different parameters of the chirped grating lens, such as F number, interaction length  $d$  and the periodicity of the grooves.

6.3 The fabrication of chirped grating lenses on  $\text{Nb}_2\text{O}_5$  transition waveguides is an alternative method that may improve the performance of grating lenses from the point of view of obtaining both larger throughput efficiency and larger angular field of view. The deposited  $\text{Nb}_2\text{O}_5$  films on  $\text{LiNbO}_3$  have refractive indices larger than the extraordinary index of the Ti-indiffused layers in  $\text{LiNbO}_3$ . Also, the mode depth of  $\text{Nb}_2\text{O}_5$ - $\text{LiNbO}_3$  waveguides is two to three times smaller than the mode depth of Ti-

indiffused waveguides. Therefore, a much stronger interaction between the guided wave and the grating grooves is expected if the grating lenses are fabricated on  $\text{Nb}_2\text{O}_5$ - $\text{LiNbO}_3$  waveguides.

The fabrication of  $\text{Nb}_2\text{O}_5$ - $\text{LiNbO}_3$  waveguides by the reactive sputtering of  $\text{Nb}_2\text{O}_5$  films, the fabrication of low-loss transition waveguides interconnecting two regions of Ti-indiffused  $\text{LiNbO}_3$  waveguides, and the fabrication of the grating grooves on  $\text{Nb}_2\text{O}_5$  films by reactive ion beam etching and  $\text{TiO}_2$  deposition have been investigated.

Very low-loss  $\text{Nb}_2\text{O}_5$  transition waveguides with a total insertion loss of 0.8 dB have been demonstrated. The key to low-loss transition is a very smooth taper obtained through a glass shadowing mask during the deposition of the  $\text{Nb}_2\text{O}_5$  film. Chirped grating lenses also have been fabricated on  $\text{Nb}_2\text{O}_5$  waveguides that yield an 85% throughput efficiency and four degrees angular field of view. Thus, by combining the tapered transition and the grating lens, it is possible to obtain the lens function with a high efficiency and a large angular field of view for any signal processing application using Ti-indiffused  $\text{LiNbO}_3$  waveguides without the disadvantages of the deep mode depth and small  $n_{\text{eff}} - n_{\text{sub}}$  values. However, this fabrication technique has several drawbacks.

1. The loss of the transition waveguide increases as the direction of propagation is moved away from the ordinary axis of the  $\text{LiNbO}_3$  crystal because the ordinary index of  $\text{LiNbO}_3$  is larger than the index of the  $\text{Nb}_2\text{O}_5$  film.
2. The  $\text{Nb}_2\text{O}_5$  waveguide is affected severely by any processing that involves temperatures higher than 200°C.

3. The  $\text{Nb}_2\text{O}_5$  transition introduces  $\approx 10$  dB of inplane scattered noise in addition to the inplane scattered noise of the Ti-indiffused  $\text{LiNbO}_3$  waveguide.

Therefore, we conclude that for applications such as the integrated optic spectrum analyzer, further research is required to: (a) improve the uniformity of the tapered edges of the transition waveguide in order to reduce the inplane scattering caused by the tapered edges; (b) optimize the tapered slope and length for minimum transition loss; and (c) investigate the performance of transition waveguides fabricated by materials with refractive indices higher than that of  $\text{Nb}_2\text{O}_5$  films, such as  $\text{TiO}_2$  and  $\text{As}_2\text{S}_3$ .

6.4 The fabrication of grating lenses on ion exchanged  $\text{LiNbO}_3$  waveguides is the second alternative that has been investigated in order to improve the grating lens performance and relax the limitation imposed by the properties of Ti-indiffused  $\text{LiNbO}_3$  waveguides. The ion exchanged layer in  $\text{LiNbO}_3$  has a refractive index of 2.32 which is large compared to the substrate index of 2.20.

Double ion exchanged chirped grating lenses in  $\text{LiNbO}_3$  waveguides have been fabricated and a throughput efficiency of 75% and three degrees angular field of view have been measured for some lenses. It is potentially feasible to obtain higher efficiency and larger angular field of view by using a grating lens structure of small  $d$  length. However, there are several drawbacks in using ion exchanged waveguides.

1. The inplane scattering loss of the ion exchanged waveguide is considerably larger than the Ti-indiffused  $\text{LiNbO}_3$  and  $\text{Nb}_2\text{O}_5$ - $\text{LiNbO}_3$  waveguides.
2. The ion exchanged waveguide is affected by processes that involve temperatures higher than  $200^\circ\text{C}$
3. The lateral diffusion caused by the ion exchange process may be a limiting factor in the effectiveness of this process for small periodicity structures.

In order to assess the effectiveness of ion exchanged waveguides for integrated optic signal processing applications, further research is required to: (a) reduce the inplane scattering of these waveguides; (b) investigate the lateral diffusion of the ion exchange process; and (c) investigate the stability of such waveguides due to aging.

In short, efficient chirped grating lenses on Ti-indiffused  $\text{LiNbO}_3$  have been fabricated successfully. The limitations in performance of the grating lenses on such waveguides have been investigated. Two alternative material structures have been investigated that can circumvent the difficulties with Ti-indiffused  $\text{LiNbO}_3$  waveguides. Furthermore, the limitations of each structure has been determined.

## CHAPTER VII

## APPENDIX I.

This appendix is devoted to the design and analysis of chirped grating lenses by the generalized coupled mode analysis [1]. The appendix is subdivided into two parts. In the first part it is shown how this analysis may be used to design curved and chirped quasi-periodic structures for obtaining phase match interactions between two specific guided wave beams. In the second part, the type of design information (e.g., diffraction efficiency, diffracted spot size, angular field of view, etc.) that has been obtained by this analysis is demonstrated in a few examples.

## A. Generalized Phase Matched Diffraction

In the generalized coupled mode analysis, it is assumed that only two guided wave beams are coupled to each other via the chirped or curved grating structure (Figure 1), i.e., the Q factor of the grating is high enough so that diffraction into the higher order is negligible. In this analysis, the electric and magnetic fields of the incident and diffracted guided wave modes are expressed as a product of three functions in the form

$$E_i = P(x,y) \psi_i(x,y) F(z) \quad (1)$$

$$E_d = Q(x,y) \psi_d(x,y) F(z) \quad (2)$$

where  $P(x,y)$  and  $Q(x,y)$  are the slow varying amplitude and phase functions